GEORG-AUGUST-UNIVERSITÄT
GÖTTINGEN

Axonemal dyneins and force generation

by neurons in *Drosophila melanogaster* ear.

Dissertation
for the award of the degree

"Doctor rerum naturalium"
of the Georg-August-Universität Göttingen

within the doctoral program *(Sensory and Motor Neuroscience)*

of the Georg-August University School of Science (GAUSS)

submitted by

Somdatta Karak

from West Bengal, India

Göttingen 2013

Thesis Committee

Prof. Dr. Martin Göpfert

Georg-August-University Göttingen, Cellular Neurobiology.

Prof. Dr. André Fiala,

Georg-August-University Göttingen, Molecular Neurobiology of Behavior.

Prof. Dr. Tobias Moser,

Georg-August-University Göttingen, Medical Centre.

Members of the Examination Board

Referee: Prof. Dr. Martin Göpfert, Georg-August-University Göttingen, Cellular Neurobiology.

2nd Referee: Prof. Dr. André Fiala, Georg-August-University Göttingen, Molecular Neurobiology of Behavior.

Further members of the Examination Board

Prof. Dr. Tobias Moser, Georg-August-University Göttingen, Medical Centre.

Prof. Dr. Gregor Eichele, Max Planck Institute of Biophysical Chemistry, Department of Genes and Behavior.

Dr. Henrik Bringmann, Max Planck Institute of Biophysical Chemistry.

Dr. Camin Dean, European Neuroscience Institute.

Date of oral examination: .28.10.2013

Declaration.

I herewith declare that the PhD thesis entitled “Axonemal dyneins and force generation by neurons in Drosophila melanogaster ear” has been written independently and with no other sources and aids other than quoted.

Somdatta Karak

Göttingen, 31st August, 2013.

Table of Content.

Table of Figures.

List of Tables.

1. Introduction

Mechanotransduction is conversion of any form of mechanical stimuli into electrical signals. This includes detection of vibrations, pressure changes, touch- both gentle and harsh, gravity and temperature. It is, thus, involved in every complex behavior displayed by an animal and is instrumental in an animal's perception of its surroundings. Metazoans employ specialized mechanosensory organs for detection of each of these different physical stimuli. These mechanosensory organs are structurally organized and positioned on the body in a way to facilitate effective detection of specific stimuli. In addition to structural specializations, the sensory organs can also be differentiated on the basis of protein expression in these neurons. One of the most widely studied proteins in the mechanosensory organs has been the ion channels expressed by these sensory neurons mainly due to the relevance in dealing with sensory disorders. Various Transient Receptor Potential (TRP) superfamily ion channels have been implicated in mechanosensory neurons and studies have shown that different mechanosensory systems utilize different ion channels. However, a complete understanding of the molecular mechanisms of mechanotransduction has remained elusive for a long time and is still considered one of the most intriguing questions in sensory biology. Lately numerous studies have shown parallels between the mechanotransduction mechanisms in vertebrates and invertebrates. Coupled with the ease of handling, genetic manipulations and *in vivo* physiological studies it makes *Drosophila melanogaster* attractive model system to study mechanotransduction and still be able to use the findings to understand the vertebrate ear better.

1.1 Mechanosensation in Drosophila melanogaster:

Flies utilize two basic types of mechanosensory organs: 1. Type I organs that are multicellular comprising 1-4 sensory neurons, surrounded by specialized support cells. The sensory neurons show a single dendrite with a modified cilium. 2. Type II organs that comprise single, non-ciliated multidendritic (md) neurons with different degrees of dendritic arborizations and no associated support cells. Type I organs can be further

classified into external sensory (es) organs and chordotonal (ch) organs. Es organs, as the name suggests, have external cuticular parts that are deformed by mechanical stimuli (Dickinson, 1999) while the ch organs lack external structures and are situated beneath the cuticle (Yack, 2004). Es organs include two types of sensilla, bristles and campaniform sensilla. Bristles possess a curved bristle shaft seated in a socket. Deformations of the bristle shaft are detected by a single sensory neuron. Campaniform sensilla, by constrast, display a cuticular dome instead of a bristle shaft. This dome is compressed by cuticular stretch. The ch organs are innervated by stretch-sensitive ciliated sensory neurons enclosed in a scolopale space with a dendritic cap at its distal tip that attaches with the cap cell (Fig. 1d and e) (Hartenstein, 1988; Yack, 2004). Mechanical stimuli are conveyed to the neurons via the cap cell.

The different types of mechanosensory organs are differentially placed to suit their respective function. Bristles are abundantly present on the fly body, including numerous macrochaetes and microchaetes on head and thorax, legs, wings and hair plates to detect touch and changes in joint positions and are the most important proprioceptors in flies. They are also present on the mouthparts where they serve a contact chemosensory function. Campaniform sensilla are situated at limb joints, the base of halteres and wings, and along the wing blade. They detect the change in angular momentum during flight via detection of the gyroscopic forces generated at the base of wings and halteres. Ch organs act as touch receptors and proprioceptors in larvae as they are situated in the body wall. The two most prominent ch organs in adults are Johnston's organ (JO) in the second segment of antenna and femoral chordotonal organ (FCO) in each leg. Different neuronal populations in JO detect various stimuli, eg. air-driven vibrations due to near-field sound sources, wind and gravity (Kamikouchi *et al*, 2009). The FCO, by contrast, detects flexion of the femoral joint (Kamikouchi *et al*, 2010). Md neurons are internally located and innervate trachea and various regions of body wall. The varied morphologies and internal location of md neurons have made it more difficult to assign functions to these neurons. However, recent studies have demonstrated that md neurons not only play a role in proprioception but also in detection of pain (Ainsley *et al*, 2003, Zhong *et al*, 2010).

Though the overall cell lineage and fate determination in development of different mechanosensory organs is similar, different transcription factors are required for the

development and the differentiation of the sensory organ precursor cells into sensory neurons and the support cells (Fichelson & Gho, 2003, Orgogozo *et al*, 2002, Lai & Orgogozo, 2004). The *achete scute* complex is required for the differentiation of es organs (Campuzano and Modollel, 1992) while *atonal* inhibition on this pathway results in the formation of ch organs (Jarman *et al*, 1993, Jarman *et al*, 1995, Cachero *et al*, 2011). One of the most striking structural differences observed in the ch organ neurons is the presence of a rather long ciliated dendrite that bears a swelling at half its length, called the ciliary dilation. The cilium shows a microtubular doublet structure with axonemal dynein arm-like protrusions spanning from the base of dendrite to the ciliary dilation. In the distal part of the neurons beyond the ciliary dilation, the microtubular organization becomes random with no dynein-like arms (Fig. 1f-h, data provided by Dr. Maike Kittelmann). The es neurons, on the other hand, show only a short connecting cilium that extends distally into a tubular body (reviewed in Kernan, 2007). The tubular body is formed of a bunch of tightly arranged microtubules, placed adjacent to each other with no dynein-like arms.

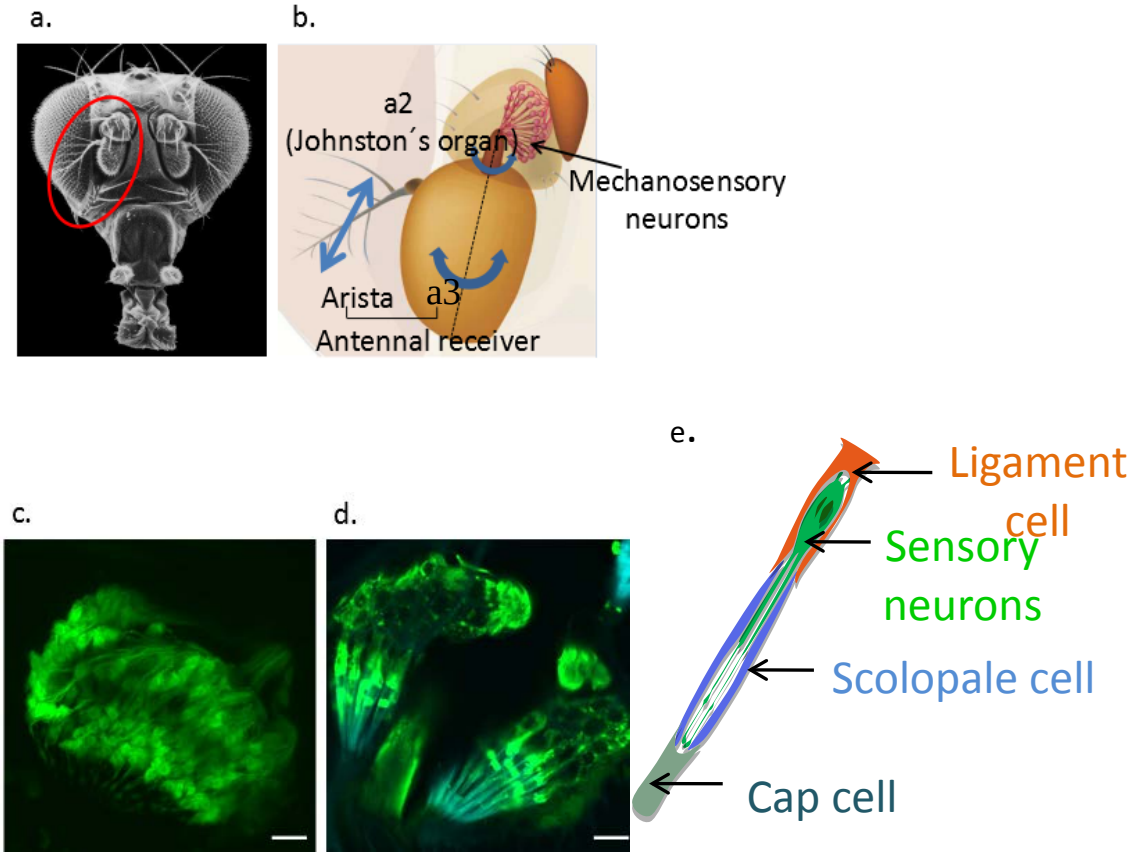

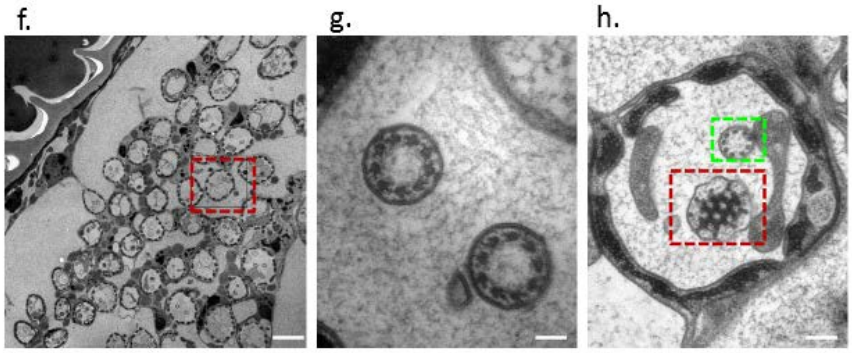

Fig. 1.1: Anatomy of fly ear. a and b:The fly ear comprises a pair of tripartite antenna with an arista projecting from each third segment, a3. The arista with the a3 acts as the sound receiver and activates the mechanosensory neurons housed in the a2 (b: Kamikouchi *et al*, 2009). c, d and e: Arrangement of JO neurons. c shows JO neurons marked by promoter fusion construct of a ch organ specific gene (*CG6053*). d shows JO neurons marked by horseradish peroxidase (HRP) in green and scolopale cells by actin staining using phalloidin in blue. Scale bar: 10 µm. e. shows schematic of scolopidium, functional unit of JO (e: Bechstedt *et al*, 2010). f, g and h: Ultrastructure of JO neurons. Electron microscopic analyses shows the ultrastructure of the JO neurons. The red box in f shows cross-section of a single scolopidium. The enlarged pictures of a single scolopidium are shown in fig. g and h. Each scolopidium contains 2-3 sensory neurons. Scale bar: 2 µm. g. Cross-section of JO neurons at the proximal outer dendritic region. This region of the JO neurons show a microtubular axonemal structure with dynein-like arms. Scale bar: 100 nm. h. Towards the distal end the cross-sections show an electron dense structure (shown in red box) called the ciliary dilation. From the ciliary dilation to further towards the tip the microtubular arrangement loses the dynein arms. Scale bar: 200 nm.

The only other ciliated cells reported in flies are the motile sperm cells (Kavlie *et al*, 2010). Though the ch organ neurons show primary cilia with no central pair of microtubules, a feature seen in many non-motile cilia (Kavlie *et al*, 2010), presence of dynein-like arms is believed to endow the neurons with active motility. This proposed idea forms a strong basis to explain the active antennal mechanics seen in fly hearing.

1.1.1 Neuronal basis of hearing:

1.1.1.1 In *Drosophila melanogaster*:

As already aforementioned the JO neurons detect near-field sound stimuli, wind and gravity. The different neuronal populations that detect sound and wind and gravity are spatially demarcated and molecularly recognizable in JO.

The fly arista and third antennal segment, the funiculus act together as the sound receiver and rotate along a longitudinal axis about the second antennal segment, the pedicel (Fig. 1a-b). The pedicel houses about 200 functional units called scolopidia (Fig. 1c-e). Each scolopidium contains 2-3 sensory neurons enclosed in a scolopale space. This space, which is formed by scolopale cells contains a potassium-rich receptor lymph. The scolopale cells converge at the distal end of the neurons and secrete NOMPA, a matrix

protein that forms the dendritic cap at the distal tip of the neurons (Chung *et al*, 2001). The dendritic cap attaches the cilia to the cap cell, which is connected via a hook to the funiculus. The cap cell thus, forms the connection via which the mechanical stimuli are carried to the mechanosensory neurons.

The JO neurons show sound-evoked compound action potentials (CAP) with a delay of microseconds (Albert et al, 2007) that is too fast for a second-messenger cascade. This indicates that JO neurons detect mechanical stimuli via directly-gated mechanotransduction channels. Opening of directly gated mechanosensitive ion channels is also reflected by antennal mechanics.

The antennal movements can be monitored non-invasively by laser Doppler vibometry where a low power laser is focused on the arista (Göpfert & Robert, 2002). Movement of the arista causes a change in the interference of the incident and reflected light which is detected by the vibrometer and gives a measure of the velocity of the movement. The velocity information can then be used to measure the aristal/ antennal displacement and the power spectrum of the system. Fly antennae show spontaneous oscillations much like the vertebrate hair cells in the cochlea. When Fourier transformed the velocity trace can be converted from its time domain into its frequency domain and can be used to study the frequency tuning of the antennae. It shows that though the antennae are broadly tuned to frequencies upto several hundred Hz, the measures of antennal velocity are the highest at around 250Hz. When sine stimuli are applied at this frequency, nonlinear active amplification is observed for low intensity stimuli. The sound-evoked CAP responses show a frequency doubling suggesting that JO neurons are tuned to the frequency of spontaneous oscillations/ free fluctuations seen in the antennae. It also suggests that there are two opposing populations of JO neurons which detect the two different phases of the sine stimulus.

1.1.1.2 Parallels with vertebrate hearing*:*

The well-studied mammalian ear consists of an outer, middle and inner ear (Slepecky, 1996). The outer ear funnels sound into the middle and inner ear via various fluid-filled compartments where it causes production of pressure waves. The structure of the inner ear or the cochlea is such that the base of the cochlea vibrates with high frequency and

with gradually decreasing frequencies towards the apex, thus generating the first level of tonotopicity in the auditory system. These waves are detected by the auditory sensory cells situated in the organ of Corti placed on the basilar membrane. The sound waves result in the movement of the tufts of stereocilia protruding from the apical surfaces of the auditory sensory cells. However, notwithstanding the different anatomies of the sound receivers in vertebrates and invertebrates, they share similar mechanical properties as: 1. Frequency selective cycle by cycle amplification of vibrations. 2. Compressive nonlinearity that makes the ear particularly sensitive to low intensity sounds. 3. Power gain via active processes in the system and 4. Spontaneous self-sustained oscillations (Ruggero & Rich, 1991, Ruggero, 1997, Manley & Köppl, 1998, Göpfert & Robert, 2002).

1.1.2 Theoretical understanding of the ear mechanics:

The mechanical properties in both vertebrate and invertebrate ear match those of a dynamic system operating near the critical point of Hopf bifurcation (Choe et al., 1998; Camalet et al., 2000; Eguilúz et al., 2000). The critical point separates two regimes, stable and oscillating. A slight change in a control parameter can shift the system from one regime to another. On the stable side of Hopf bifurcation the system will produce the first three characteristics, viz. frequency selectivity, amplification and compressive nonlinearity whereas self-sustained spontaneous oscillations arise on the other side of the bifurcation. To oscillate and actively amplify inputs a system should be coupled to a power source. A system operating at Hopf bifurcation is not only endowed with the ability to amplify its inputs but also displays phase locking property. This enables the ear to detect new stimulus by adjusting itself to the phase of the stimulus. For the most optimum performance the auditory system needs to be poised near the critical point. A negative feedback is required to maintain the system constantly around this point.

Theoretical studies explain these properties by a two-state gating spring model (Hudspeth *et al*, 2000, Nadrowski *et al*, 2008). The model posits a series arrangement of gating spring, ion channel (which is either completely open or closed) and adaptation motors in the mechanosensory auditory neurons/ hair cells. The gating springs maintain the stiffness of the system, which is regulated by the opening of ion channels. Ion channels

have an open probability of nearly 0.5. Opening of ion channels relaxes the spring and thus, the stiffness of the system drops. At the same time influx of ions, presumably of $Ca^{+2,}$ causes activation of adaptation motors. Adaptation motors move the complete transduction machinery in the direction of closure of ion channels to restore the open probability of ion channels back to 0.5 and the system adapts to enable detection of new stimuli. As the whole transduction machinery moves this displacement is taken up by the antennae/ the hair cells since the ion channels are directly gated by the sound receiver. The interplay between ion channels and adaptation motors provides the neurons with an intrinsic property of energy conversion in the system, similar to cochlear amplifier in vertebrate ears. This further leads into a positive feedback that amplifies the inputs. This is reflected in larger antennal/ hair cell movements. Since work is done by the system, output exceeds input causing power gain in the system. However, under higher sound intensity conditions, the movements of adaptation motors reach their saturating limit and no more power gain is observed in the system.

At rest the spontaneous opening and closing of ion channels is sufficient to cause movement of the adaptation motors and thus give rise to self-sustained oscillations while maintaining the open probability of ion channels constant at around 0.5.

1.1.3 Molecular basis of hearing:

1.1.3.1 In invertebrates:

Spontaneous oscillations and non-linear mechanics of antennae are independent of synaptic transmission from the JO neurons. Thus, these are intrinsic properties of the JO neurons and arise from the molecular process of mechanotransduction. Mutation in *nompA* disrups the connection between the distal end of cilium and the cap cell. These mutant antennae do not oscillate and show a decreased resonant frequency (Göpfert & Robert, 2003). Thus, the connection of the neurons with the funiculus is required to observe activity in the antennal mechanics. *Rfx* and *fd3f* mutants which lack cilia in the JO neurons show lack of active antennal mechanics (Cachero *et al*, 2011, Newton *et al*, 2012). Mutation in TilB, a protein required for ciliary assembly disrupts axonemal dynein arms in JO neurons and sperm tails, resulting in loss of active amplification in the

JO neurons and sperm immotility (Kavlie *et al*, 2010). Thus, the presence of axonemal dyneins in the cilia of JO neurons is required for motility in these neurons.

There are at least two populations of ion channels of the TRP superfamily that are expressed in JO neurons, No mechanotransducing Potential C/ NOMPC (TRPN1) and Nanchung/ NAN and Inactive/ IAV (TRPV), which presumably form a heterodimeric NAN-IAV channel (Gong *et al*, 2003, Liang *et al*, 2011, Effertz *et al*, 2011, Lehnert *et al*, 2012). The expression of ion channels is spatially separated in the JO neurons. NAN and IAV are expressed together in the outer dendritic region of the JO neurons proximal to the ciliary dilation (Gong *et al*, 2003). NOMPC is expressed at the distal end of the cilium, beyond the ciliary dilation (Liang *et al*, 2011). *NompC* mutants lack active antennal mechanics but still retain a remnant sound-evoked action potential response from the antennal nerve (Effertz *et al*, 2011). *Nan-iav* mutants, by constrast, show higher antennal oscillations and excess amplification but lack sound-evoked CAP responses (Göpfert *et al*, 2006). Active antennal mechanics are also abolished in *nompC* and *nan* double mutants (Göpfert *et al*, 2006). Taken together this suggests a role for NOMPC as a mechanotransducing channel. But the remnant CAP responses hint at the presence of other mechanotransducing ion channel populations as well. While the mechanotransducing machinery is still intact in the TRPV mutants, which is evident from the antennal mechanics, the negative feedback on the mechanics is lost. Also the initial receptor potential from the mechanotransducing machinery might be too small to be detected as neuronal action potentials in the TRPV mutants. TRPV channels, thus, seem to function in amplification of the initial sound-evoked receptor potential.

Since NOMPC is expressed at the distal end of the cilia it seems plausible that it might be activated mechanically due to stretch on the neurons. TRPV channels expressed in the proximal region might still be mechanically gated by the membrane tension or by influx of ions from the TRPN1 (NOMPC) channels. Studies in mammalian TRPV channels have shown that they bind to microtubules in a Ca^{+2} dependent manner (Goswami *et al*, 2004). Similar mechanisms might operate in the TRPV channels of ch neurons as well and thus making it possible for the TRPV channels to detect the changes in the tension of axonemes.

Pharmacological disruption of the microtubular structure in the cilia of JO neurons in mosquito *Culex quinquefasciatus* using colchicines, abolishes active amplification (Warren *et al*, 2010). The same study showed that the energetics of active amplification in a mosquito ear matches with a dynein-powered system. However, colchicine treatment can also affect the integrity of the neurons (Goldschmidt & Steward, 1989) or the molecular mechanisms required for active amplification. The non-specificity of the pharmacological techniques necessitates it to address the question using more specific genetic manipulations.

1.1.3.2 In vertebrates:

The identity of mechanotransducing ion channel that acts in vertebrate hair cells has remained elusive as NOMPC does not have a mammalian homolog. Recent studies hint towards the role of TMC1 and TMC2 in mechanotransduction in mice hair cells (Kawashima *et al*, 2011, Pan *et al*, 2013). Hair cells use actin-based cytoskeletal structures called the stereocilia as the transducing sites (reviewed in Peng *et al*, 2011). Myosins are, hence, believed to act analogous to ciliary motors in the hair cells. Myosin-1c has been suggested though debatable as possible motors in the mammalian hair cells (Cyr *et al*, 2002, Holt *et al*, 2002, reviewed in Gillespie 2004). In addition to myosins, prestin-driven electromotility drives active amplification in mammalian ear (Nin *et al*, 2012). Prestin belongs to an anion transporter family, the solute carrier protein 26A (SLC26A). A motif of eleven amino acids, called the MESH motif in mammalian prestin endows it with the voltage-dependent motility (Tan *et al*, 2012). It is predicted that it is this MESH motif present only in eutherian prestin that facilitates internal charge movement and translates into conformational changes in the molecule which thus results in somatic motility. However, prestin in non-eutherian animals lack the MESH motif and do not show motor functions.

1.2 Aim of thesis:

Given that it is much faster to genetically manipulate the fly auditory system than in vertebrates and *in vivo* studies are much easier in invertebrates, it makes it more attractive to understand force generation in JO neurons of fly antenna. The hypothesis tested in this

thesis is that axonemal dyneins in the cilia of JO neurons act with ion channels to generate force required for the antennal mechanics observed. The genetic and molecular mechanisms supporting this argument will be discussed in this thesis.

1.2.1 Structure and functions of axonemal dyneins:

Unlike cytoplasmic dyneins that act as retrograde molecular motors (Pederson and Christinsen 2012), axonemal dyneins are known to confer motility in ciliary and flagellar structures (King 2013). As the name suggests axonemal dyneins are present in axonemal microtubular structures. Motile axonemes are formed by 18 outer microtubules and 2 central ones in most of the cases (Minzuno *et al*, 2012). However, there are examples like nodal cilia which have motile axonemes and lack the central pair of microtubules (Hirokawa *et al*, 2009). The outer microtubules exist as 9 doublets, each consisting of α and ß tubulin. Outer and inner arm axonemal dyneins, named so according to their location within the cilia, are bound to the microtubular structure and confer ciliary bending and motility. Previous studies have shown that outer arm dyneins control slide velocity of microtubule and thus, determine ciliary beat frequency whereas inner arm dyneins determine beat form (parameters like the amplitude of the beat).

Each outer and inner arm axonemal dynein is a multi-protein complex formed by 1-3 axonemal dynein heavy chains, 1-2 intermediate chains and several light intermediate and light chains (Höök and Vallee, 2006, King, 2013). The head of the axonemal dynein arms is formed by the heavy chains and might be a homomer or heteromer. The heavy chains possess a microtubule binding domain and upto 6 ATPase domains (Roberts *et al*, 2012). The head of the dynein arm is attached to α-tubulin. Intermediate chains have WD40 domains which are seen in proteins that act as adaptor molecules. WD40 domains are important in the formation of functional protein complexes. The axonemal light chains are bound to the intermediate chains and face the ß-tubulin. The ATPase domains of the axonemal heavy chain confer the property of conversion of chemical energy into mechanical energy via ATP hydrolysis. This energy is utilized for generating an active stroke by the dynein arm that causes sliding of adjacent microtubules with respect to each other and gives rise to ciliary bending. Such axonemal dynamics are pivotal for ciliary and flagellar movements.

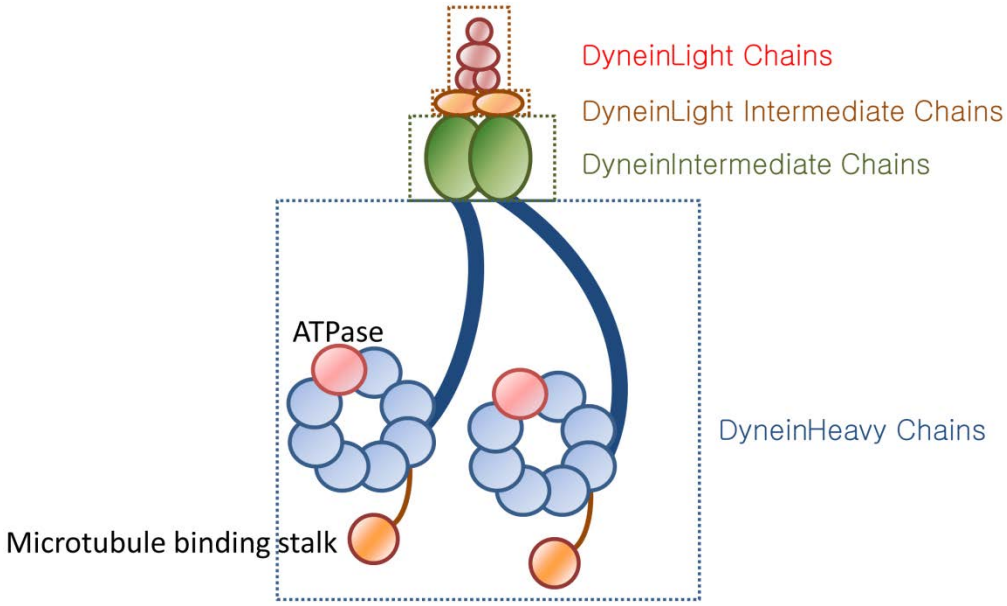

Fig. 1.2: Molecular arrangement of an axonemal dynein complex (modified from Mallik and Gross, 2004). Axonemal dynein arm is a multi-protein complex present only in the microtubular structures. It is formed by 1-3 dynein heavy chains, 1-2 dynein intermediate chains and several light intermediate chains and light chains. The dynein heavy chain binds to the microtubules in the axoneme and hydrolyses ATP via its ATPase domain to produce energy. This energy is used for ciliary and flagellar movements. The other components in the complex act as adaptor and regulator molecules to ensure proper formation and functioning of the complex.

The ch neurons show ciliated axonemes with dynein arms but lack the central pair of microtubules. It is only rational to check how the motile axonemes can generate force using dyneins as molecular motors. It would be interesting to deduce the molecular mechanisms of axonemal dynein activity in the JO neurons and decipher the different aspects in the JO neuronal functioning that are controlled by ciliary motility. This thesis will try to address each of these questions with sufficient details.

2. Materials and Methods.

2.1 Generation of fly stocks/ transgenic fly lines:

2.1.1 UAS-GAL4 strategy:

Transgenic fly lines are available for the various *UAS* and *Gal4* stocks in Bloomington. The *Gal4* lines are made such that GAL4 is expressed under the promoter of interest. The *UAS* lines are made to enable over-expression of the protein of interest under the Upstream Activating Sequence (*UAS*) which is activated by presence of GAL4. The transgenes containing the *Gal4* and *UAS* constructs are hence put together in a fly stock to over-express a protein of interest under the control of promoter of choice (or in a tissue specific manner). Simply crossing males of one of the two transgenic lines with virgin females of the other enables to obtain progeny that contains both the transgenic lines.

2.1.2 Excision of Minos insertions:

The Minos insertions in the genes *CG17150* and *CG6053* are precisely excised out genetically using Minos transposase. Minos transposase is transgenically induced under heat shock promoter at 37°C. The fly vials are kept in a water bath maintained at 37°C for 1 hr daily until pupariation. Expression of transposase enables excision of the Minos element. The precision of the excision lines obtained is confirmed by performing PCR using genomic DNA of the flies as DNA template, TOPO cloning the PCR product followed by DNA sequencing to validate the absence of Minos insertion in the genome of the flies after the genetic manipulation and that the fly lines have retained back the original reading frame of the respective genes.

The regions of interest checked for the absence of Minos insertion were amplified by PCR using the following primers in the precise excision flies generated for *CG17150* and *CG6053* mutant lines.

CG17150:
Forward: 5'-CCGTGTGTTGCTCCGTATCCTTC-3',

5’-CTAATCGAATCCTTAGGTCGGCAG-3’ (positive control)
Reverse: 5’-CTACGCTACACTAAGTTGGAACG-3’,
5’-CGAAGCAGTGTTGCCAATTCATCC-3’ (positive control)

CG6053:
Forward: 5’-CCTCACTGAGTGTGGCCAATACGG-3’,
5’-CCTGAAACTCAGACGGCGTCTAAC-3’ (positive control),
5’-AAGGCCAACCATGGCCAGGATC-3’ (positive control)
Reverse: 5’-CTCTGCAATCCTCCGACCAGATTCG-3’,
5’-TTGATGCCACACGTCTGATCTACGG-3’ (positive control),
5’- AGTAGAACTCGGATCGTTCGATACC-3’ (positive control)
The PCR products obtained thus were then cloned into TOPO vectors so that the DNA sequence of interest could be even further amplified and hence, facilitate easier DNA sequencing. The primers used for sequencing the DNA products post-TOPO cloning are 5'- GAT TTA GGT GAC ACT ATA G -3' (SP6 end) and 5'- TAA TAC GAC TCA CTA TAG GG -3' (T7 end).

2.1.3 CG6053 genomic rescue:

A BACPAC clone no. CH322-70G22 from P(acman) resource centre was obtained which contains a 20kb region spanning *11683101 to 11705106* of chromosome arm 3L of a wild type fly which includes the complete genomic region of *CG6053* (which spans from 11690438 to 11692363 on chromosome arm 3L).
Qiagen Plasmid Midi kit used to extract DNA from this BACPAC clone.
A colony picked from a freshly streaked plate with the bacterial suspension of the (CH322-70G22) BACPAC clone is grown overnight at 37°C with vigorous shaking. The bacterial cells are then harvested by centrifugation at 6000g for 15min at 4°C. The pellet is then resuspended in 20mL buffer P1 followed by addition of 20mL of buffer P2 and thoroughly mixed by inverting the sealed tube 4-6 times. It is then incubated at room temperature (about 20°C) for 5 min. 20mL of chilled buffer P3 is then added, mixed immediately and thoroughly by inverting the tube 4-6 times and incubated on ice for 30min. The mixture is then centrifuged at ≥20000g (how much exactly) for 30 min at 4°C. The supernatant is promptly removed and transferred to a new 50 mL falcon tube. The supernatant is centrifuged again at ≥20000g for 15 min at 4°C. The supernatant is then removed immediately and 42mL isopropanol is added to this lysate to precipitate the DNA. The mixture is centrifuged at ≥15000g for 30 min at 4°C and the supernatant is

carefully removed the DNA pellet. The pellet is then resuspended in 500µL TE buffer and buffer QBT is then added to obtain a final volume of 5mL. In the meanwhile the resin to be used for DNA binding (Qiagen tip 100, provided in the kit) is equilibrated by allowing 4mL of buffer QBT to empty through it by gravity flow. The DNA solution is then added onto the resin and allowed to flow through it under gravity. The Qiagen tip is then washed twice with 10mL buffer QC and eluted with 5mL buffer QF.

Purification: The DNA in the elute is then precipitated by addition of 3.5 mL isopropanol at room temperature and then centrifuged at 15000g for 30 min at 4°C. The DNA pellet is then washed with 70% ethanol and centrifuged at 15000g for 10 min. The supernatant is carefully decanted without disturbing the pellet. The pellet is allowed to air dry for 5-10 min and then redissolved in 2 mL of TE buffer, pH 8.0.

The DNA sequence of the insert in the BACPAC clone was checked with primers: 5'-AAGAGCAGTCAAATATTTTGCTAAGTTTCC-3' & 5'-GGATACCAGGAAGCTTACCGAACC-3'.
The BAC clones were microinjected into w^{1118} by BestGene.

2.1.4 Cloning transgenic constructs:

a. *CG6053* Gal4

Genomic DNA from wild type flies was used as DNA template with the following primers to amplify the promoter region of *CG6053*.
Forward: 5'-CGAATTCAAATCAAACCAGCTCTTGTAGTTACC-3'
Reverse: 5'-CGGATCCGAGTTCTCGGTGAACACCACCT-3'
The DNA product was generated such that it was flanked by EcoR1 and BamH1 sites on the 5' and 3' ends respectively.

b. UAS CG6053

DGRC clone no. IP13643 was obtained which contains *CG6053* cDNA flanked by Ase1 sites

in pOT2 vector. The clone was retransformed into (what strain of bacteria) and genomic DNA was obtained from the colonies to check the DNA sequence of CG6053 cDNA with the primer 5'-CGTTAGAACGCGGCTACAATTAATAC-3'

The following primers were used to amplify the insert from the IP13643 and then maintained in TOPO vector.

Forward: 5'-CCGAATTCAAATATTTTGCTAAGTTTCCGATTGAAATGGAA-3'
Reverse: 5'-GATCTAGACAGCCTCCTCCGCATCCTCTAC-3'

EcoR1 and Eag1 are used to excise out the 1659 bps of CG6053 cDNA sequence and ligate into UASTattb vector.

c. *UAS CG6053* YFP

The following primers were used to amplify YFP from an existing vector such that the 5' end of YFP was now flanked by Eag1 and the 3' end by Xba1:

Forward: 5'-TTCGGCCGGAATGGTGAGCAAGGGCGAGGAG-3'
Reverse: 5'-GGTCTAGAGCTCTTGTACAGCTCGTCCATGCC-3'

Eag1 and Xba1 were used to ligate YFP into the existing UASTattb (obtained from Baseler lab in University of Zürich) vector containing the first 1659 bps of *CG6053* transcript sequence.

The various molecular biology steps followed in the generation of the fly lines aforementioned are listed and described below.

a. Nucleic acid extraction from whole flies and bacterial cells:

i. Genomic DNA extraction from whole animals:

Whole flies are homogenized in the Qiagen TissueLyse LT homogenizer in a 1.5mL microcentrifuge tube at room temperature.

The following steps were carried out according to the Qiagen protocol for purification of total DNA from insects using the DNeasy Blood and Tissue kit.

To make a homogenate of about 10-15 flies 180µL of buffer ATL and 20µL of proteinase K are added. They are mixed thoroughly by vortexing and incubated in

a thermomixer at 56°C overnight. 200µL of buffer AL is then added and mixed thoroughly again followed by addition of 200µL of 96-100% ethanol. This mixture is then transferred into a DNeasy mini spin column placed in a 2mL collection tube (both provided in the kit) and centrifuged at 14,800 rpm for 1 min at room temperature. The flow through is discarded and 500µL of buffer AW1 is added to the spin column and centrifuged at 14,800 rpm for 1 min. The flow through is discarded again and 500µL of buffer AW2 is added to the column followed by centrifugation at 14,800 rpm for three mins. The flow through and the microcentrifuge tube are both discarded. And the spin column is then placed into a new clean 1.5mL microcentrifuge tube. 200µL of buffer AE is added to the membrane of the spin column, incubated at room temperature for 1 min and then centrifuged at 14,800 rpm for 1 min to elute the DNA sample.

ii. RNA extraction from whole flies:

The RNA extraction protocol was followed according to the ZR Tissue and Insect RNA Microprep kit by ZymoResearch.

Flies (up to 10 mg) are transferred into a ZR BashingBead Lysis Tube (provided in the kit) containing 800 µL of RNA lysis buffer and centrifuged at 14800 X g for 1 min. 400 µL of the supernatant is transferred to a Zymo-Spin IIIC Column (provided with the kit) in a collection tube and centrifuged at 8000g for 30 sec. 320 µL of 95-100% ethanol is added to the flow through in the collection tube and mixed well. The mixture is then transferred to a ZymoSpin IC Column (provided in the kit) in a collection tube and centrifuged at 14,800g for 30 sec. The flow-through is discarded and 400 µL RNA Prep Buffer (provided in the kit) is added to the column and centrifuged at 14,800g for 1 min. The flow-through is discarded. The column is then washed with 800 µL RNA Wash Buffer by centrifuging at 14,800g for 30 sec. The wash step is repeated with 400 µL RNA Wash Buffer again and the flow-throughs are discarded in both the cases. Centrifuge the column at 14,800g for 2 min to ensure complete removal of the wash buffer. The column is then placed in a DNase/ RNase free tube and 10 µL of DNase/ RNase-free water is added to the column directly, let stand for 1 min at

room temperature and centrifuged at 14,800g for 30 sec. The RNA extract obtained can be used immediately or stored at -80°C for further use.

iii. Reverse Transcription for cDNA preparation:

The RNA obtained by the above mentioned protocol is used for cDNA generation in accordance to the Quantitect Reverse Transcription protocol by Qiagen.

The RNA sample is first incubated with gDNA Wipeout Buffer (provided in the kit) at 42°C for 2 min to remove any existing genomic DNA in the sample. 1 µL Quantiscript Reverse Transcriptase, 4 µL of 5X Quantiscript RT Buffer and 1 µL Reverse Transcriptase primer mix or a polyA primer (to reverse transcribe only from mRNA in the sample) and 14 µL of template RNA are mixed well together on ice and incubated at 42°C for 15 min. Quantiscript Reverse Transcriptase is then inactivated by incubating at 95°C for 3 min. The cDNA thus obtained can be immediately used for the further purposes or stored at -20°C for long-term storage.

iv. Miniprep DNA extraction from bacterial cells:

The Invisorb Spin Plasmid Mini two kit from Stratec Molecular is used for DNA extraction from bacterial cultures of smaller quantities.

2 mL of overnight bacterial culture is transferred into a 2 mL microcentrifuge tube and centrifuged at 14,800g for 5 min. The supernatant is discarded and the pellet obtained is suspended in 250 µL cold solution A (provided with the kit). 250 µL of solution B (provided with the kit) is then added and gently but thoroughly mixed followed by 250 µL of solution C (provided with the kit). The mixture is centrifuged at 14,800g for 5 min and the supernatant is transferred onto a spin column (provided with the kit) placed in a microcentrifuge tube. It is centrifuged again at 14,800g for 1 min and the flow through is discarded. The column is washed with 750 µL of Wash solution (provided with the kit) and the flow through is discarded. The column is centrifuged again at 14,800g for 3 min to ensure complete removal of the wash solution. The spin column is placed in a new 1.5 mL microcentrifuge tube and 50-100 µL of double distilled water is added directly on the filter of the column, incubated at room temperature for 1

min and then centrifuged at 14,800g for 1 min. The elute contains DNA which can be directly used or stored at -20°C for further uses.

Determination of concentration of DNA was done by measuring the absorbance of the solution at 260nm using Nanodrop. Double distilled water was used to initialize the instrument and also as the blank solution.

b. The different PCR protocols carried out for the various purposes as mentioned above are described as follows:

i. To make the *Gal4* lines and to check the precise excisions of the Minos insertion mutants Genecraft ThermoPlus polymerase was used for performing PCR. Template DNA (max 50µg) was added with 1µL of 10mM deoxypolynucleotides (dNTPs), 1µL of 50pM of both forward and reverse primers, 2.5µL of PCR buffer, 0.5µL Genecraft thermplus polymerase and water to make the final volume of 25µL. PCR was performed using IQ Biometra professional thermocycler.

The protocol used for PCR reaction was as follows:

	STEP	TIME (min : sec)	TEMP (°C)
A	Initialization	3:00	95
B.1	Denaturation	0:30	95
B.2	Annealing	0:30	58-60
B.3	Elongation	0:30	72
C	Final elongation	7:00	72

The steps B.1, 2, 3 are repeated 35 times.

ii. For UAS line ThermoScientific Phusion polymerase was used. DGRC clone IP13643 was digested using NotI and AfeI and the DNA band of size 1.8 kb was gel extracted and used as template for PCR. Template DNA (max 50µg) was added to 1µL of 10mM dNTPs, 1µL of 50pM of both forward and reverse primers, 2.5µL of PCR buffer, 0.5µL Genecraft thermoplus polymerase and water to make the final volume of 25µL. The PCR was carried out in the BIO-RAD MyIQ thermocycler.

The protocol used to perform the PCR reaction was as follows:

	STEP	TIME (min : sec)	TEMP (°C)
A	Initialization	3:00	95
B.1	Denaturation	0:30	95
B.2	Annealing	0:30	59
B.3	Elongation	0:30	72
C	Final elongation	7:00	72

The steps B.1, 2, 3 are repeated 35 times.

iii. Gel electrophoresis: DNA samples are mixed with DNA loading buffer and are run in 1% agarose gels (for bands >500 bps) and 2% agarose gels (for bands <500 bps). 2 µL Roti-safe GelStain is added as nucleic acid stain in 50 mL of agarose solution. The gels are placed in Mini Sub Cell GT or Wide Mini Sub Cell GT electrophoresis apparatus from Bio-Rad filled with 1X TBE buffer. About 10-15µL of DNA sample in loading buffer can be loaded in each well in the gel and 5µL of the appropriate DNA ladder is loaded in one of the wells. It is connected to Bio-Rad PowerPac Basic for its power supply and the gels are run usually at 100-140V. The gels were visualized under UV light in Geliance 200 Imaging System by PerkinElmer.

iv. DNA purification:

PCR product purification/ Restriction digestion product purification: Qiagen kit: Buffer PB is added to the DNA sample in a ratio of 5:1 and mixed well. The mixture is then transferred to the spin column, provided with the kit and centrifuged at 14,800g for 1 min. The flow-through is discarded and 750µL of buffer PE is added to the column, centrifuged at 14,800g for 1 min. The flow-through is discarded again followed by a centrifugation for 3 min. The spin column is then transferred into a new 1.5mL microcentrifuge tube. 20-30 µL of double distilled water is added on the column and is incubated for 1 min at room temperature. The DNA is then eluted by centrifuging at 14,800g for 1 min.

Gel Extraction: The DNA band is cut out of the agarose gel and placed in a 2mL eppendorf tube. The weight of the agarose gel band is measured and buffer QB is added to the gel band. 100µL of buffer QB is added for every 100mg of gel. The mixture is then placed on a thermomixer at 50°C for 10 min or until the agarose gel dissolves in buffer QB. 100µL isopropanol is then added for every 100mg of gel dissolved in buffer QB. The mixture is then transferred to the minispin column provided with the kit and centrifuged at 14,800g for 1 min. The flow-through is discarded. The minispin column is then washed with 750µL of buffer QC, centrifuged at 14,800g for 1 min. The flow-through is discarded and the minispin column is centrifuged at 14,800g for 3 min. The column is then transferred to a new 1.5mL eppendorf tube and 20-30µL of double distilled water is added to the column and let to incubate at room temperature for 1 min. The DNA is then eluted out by centrifuging the column at 14,800g for 1 min.

v. Restriction Digestion: 2µL of each restriction enzyme required and 2µL of 10X FastDigest buffer are added to 0.2-5µg of DNA. Water, if required, is added to make the final reaction mixture volume to 20µL. The components are mixed gently, spun down and incubated at 37°C for 30 min. The mixture is then run on an agarose gel to check the band sizes of the restriction digestion products.

vi. Alkaline Phosphatase treatment: For insertion of DNA into plasmid vectors, vector DNA is cut with restriction digestion enzymes and then dephosphorylated. 1µL of alkaline phosphatase with 2µL of alkaline phosphatase buffer is added to the DNA to make a final volume of 20µL and incubated at 37°C for 10 min. The alkaline phosphatase is then inactivated by incubating the mixture at 65°C for 1 min.

vii. Ligation: Insert and vector DNA are added in a molar ratio of 3:1. 2µL of 10X ligation buffer and 1µL of T4 DNA ligase are added to the DNA mixture, mixed well and incubated at room temperature for 30 min.

viii. Transformation: Chemically competent cells are thawed in ice for 10 min. 5µL of ligation mixture is then added to the cells and kept in ice for 20 min more. The cells are then given a heat shock for 1 min at 42°C on a

hot plate. 200µL of autoclaved LB/ SOB medium is added to the cells and incubated at 37°C for 1 hr. The cells are then plated on agar plates with the appropriate antibiotic depending on the vector used for cloning and incubated overnight at 37°C. The vector contains gene for antibiotic resistance. Hence, only the positive clones which have the ligation product will survive on the agar plates with antibiotic and be seen as individual colonies.

ix. Preparation of new stock of chemically competent cells: The XL-1 Blue Competent Cells are thawed in ice. 20µL of the bacterial suspension is added to 5mL of SOB medium and incubated overnight at 37°C and 300 rpm. 1mL of the overnight culture is then added to 100mL of SOB medium prewarmed at 37°C and incubated at 37°C and 350 rpm for 2-3 hours until the $O.D._{600}$ of the solution reaches 0.4-0.5 as measured by a photometer. The bacterial culture is then cooled in ice for 10 min and then centrifuged at 3000 rpm at 4°C. The supernatant is discarded and the pellet is resuspended in 30mL TB buffer chilled in ice. The suspension is kept in ice for 10 min and then centrifuged at 1000 rpm at 4°C for 10 min. The supernatant is discarded and the pellet is resuspended again in 8mL TB buffer chilled in ice. 560µL of DMSO is added to the suspension and it is allowed to stand in ice for 10 min.

The suspension is aliquoted in 1.5mL microcentrifuge tubes, each containing 200µL of the suspension, frozen in liquid nitrogen and stored at -80°C for further use.

x. The positive clones are picked and grown as bacterial suspension to extract DNA by Miniprep or Midiprep as mentioned before. They can be stored in 50% glycerol at -80°C until further use.

xi. Microinjection of the cloned construct into the desired fly strain to generate the transgenic fly is performed by the company BestGene.

2.2 Fly stocks maintenance:

The fly strains are maintained at 25°C or 18°C in a 12 hr/ 12 hr light: dark cycle in plastic vials, 1/4th filled with fly food. The composition and the protocol followed to prepare the fly food are as follows:

Ingredients	Quantity (for 10L of fly food)
Agar	102g
Soya bean flour	100g
Yeast	180g
Cornmeal	800g
Treacle	220g
Malzin	800g
Propionic acid	62mL
Nipagin	150g
Ethanol	80mL

102g Agar is soaked in 5L of tap water overnight. 100g soya bean flour and 180g yeast are mixed together in 1L of tap water, 800g cornmeal in 2L of water and 220g treacle in 1L of water. All the mixtures are put together and boiled at 100°C in Varioklav® Steampot DT44580604. 800g malzin is mixed in 1L of water while 62mL propionic acid and 150g nipagin are mixed in 80mL ethanol. As the temperature of the mixture lowers to 55°C the rest of the ingredients are also added. An Isomatic MCP pump is used to fill the plastic vials with the warm food which solidifies as it cools down. The vials are fitted with mite-free plugs and can be stored at room temperature for immediate use or at 4°C for use in the next 4 weeks.

2.3 Immunohistochemistry:

The various steps followed in immunohistochemistry are mentioned as follows:

2.3.1 Fixation of antennae: The fly heads are washed once with 0.1% PBT and then fixed in 4% paraformaldehyde (PFA) for 1 hr on a rotor. Meanwhile the gelatin albumin mixture is thawed in a water bath and silicon moulds are preheated on a Medite stretching

table. The liquefied gelatin albumin mix is then put into the moulds taking care that air bubbles do not form. The fixed fly heads are then placed into the gelatin albumin mix in the moulds, cooled at 4°C for 2-3 min and the moulds are then stored in 6% PFA at 4°C overnight or until further use.

2.3.2 Vibrotome sectioning: The fly heads fixed in 6% PFA are washed in methanol for 15 min at room temperature. 40-50 μm sections of the antennae are cut using Leica vibrotome.

2.3.3 Antibody staining: The sections are washed with 1% PBT thrice, each for 15 min. It is then followed by blocking the sections in 0.25% Bovine Serum Albumin (BSA) - 10% Normal Goat Serum (NGS) mixture for 1 hr. 1° antibody is then added to the sections and kept overnight at 4°C. The sections are then washed again with 1% PBT thrice, each for 15 min followed by addition of 2° antibody. The sections are incubated in 2° antibody for 1-2 hr and washed again with 1% PBT thrice, each for 15 min. The samples are kept in DABCO for about half an hour before they are mounted on the slides using DABCO as the mounting medium.

2.3.4 Confocal microscopy: The samples were studied and imaged using the Leica laser scanning confocal microscope TCS-4D. The images were processed using image analysis software ImageJ.

2.4 Laser Doppler vibrometry:

2.4.1 Fixation of the fly for measurement: The fly is anaesthetized with CO_2 and fixed on a Teflon stand with wax and dental glue allowing movement of only of one of the antennae at the joint between the second and the third segments. The wings of the fly are clipped off. The head, the halteres, the mouth and one of the antennae of the fly are fixed with wax or dental glue.

2.4.2 Measurement of the antennal mechanics: The experimental setup is placed on an air table so prevent the environmental vibrations. Spike2.7.4 (Cambridge Electronic Design) was used to generate sound stimuli of required frequencies. An attenuator is used to regulate the intensity of the sound stimuli between 0-100dB. The frequency and the intensity of the sound stimulus detected by the fly are measured by a microphone placed near the antenna of the fly. Tungsten electrodes are used to simultaneously measure the

sound evoked compound action potential (CAP) of the antennal nerve. The recording electrode is inserted in the head region between the two antennae, the region where the antennal nerve passes through. The indifferent electrode is inserted in the thorax of the fly. The nerve signals are passed through a signal amplifier and a noise eliminator (Hum-bug, Quest Scientific). A laser point placed at the tip of the arista is traced by the Polytec PSV 400 Laser Doppler vibrometer giving a measure of velocity, displacement and one-sided power spectral density of the antenna. The antennal movements, the measurements of the microphone and CAP recordings of the antennal nerve in response to sound stimuli are converted online into fast Fourier transforms by the Polytec software.

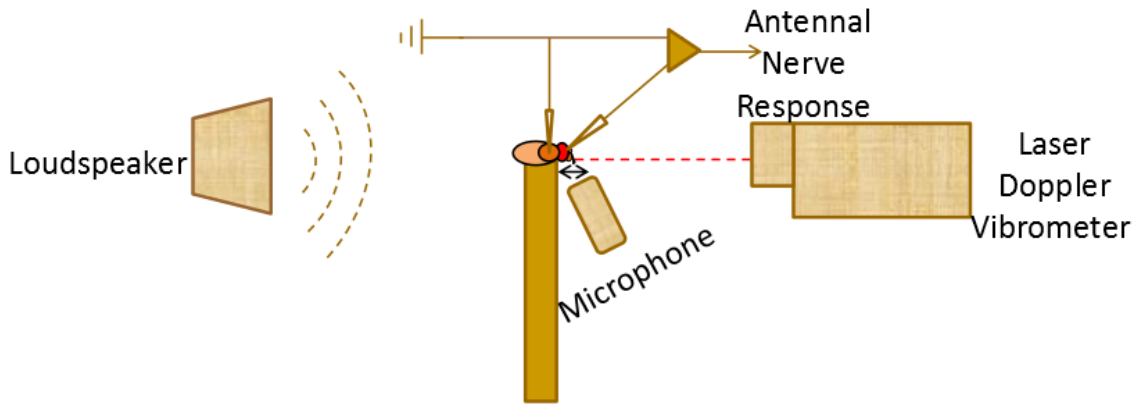

Fig. 2.1: Setup used to study antennal mechanics and sound-evoked antennal nerve response. The fly is fixed on a Teflon stand and kept such that the arista is placed perpendicular to the laser from the laser Doppler vibrometer. A loudspeaker is kept diametrically opposite to the vibrometer and is used to play the sound stimuli. A microphone is kept close to the fly arista that is being measured so that the microphone detects roughly the same intensity of sound stimuli as the fly arista. Tungsten electrodes are inserted in the fly head between the two antennae to measure the sound-evoked nerve response.

When the fly antennal movements are recorded in absence of any external specific stimulus the antenna oscillates at its individual best frequency which ranges between 150-300Hz usually for wild type flies. The further measurement of the fly antennal movements and CAP recordings are carried out by presenting sound stimuli of different intensities at the individual best frequency of the fly. The JO has two symmetric populations of neurons. Movement of the antenna in one direction causes activation of one of the populations of neurons while movement in the other direction activates the other. The CAP responses are seen at double the frequency of the stimuli presented suggesting there are two populations of JO neurons detecting two different phases of the stimuli. The CAP responses were normalized by setting the maximum CAP response for each individual fly as 1 and the least as 0. When the normalized CAP responses are

plotted against sound stimulus intensities and corresponding antennal displacements it shows a sigmoidal curve that can be fitted using a Hill equation with four parameters namely y_{min}, y_{max}, EC50 (the value of x corresponding to half the y_{max} and n (Hill slope). It can be equated as $f(x)= y_{min} + (y_{max} - y_{min})/ 1 + I x/ EC50 I^n$. The dynamic range of nerve response is calculated as the antennal displacements corresponding to 10% to 90% of the maximum CAP response.

2.5 Composition of the reagents:

2.5.1 For cloning:

2.5.1.1 Luria Broth (LB) medium: 20g LB is added to 1L double distilled water and autoclaved at 121°C.

2.5.1.2 Luria Broth agar plates: 35g LB agar is added to 1L double distilled water and autoclaved at 121°C. The molten agar is allowed to cool to about 50°C and the antibiotic desired is added and poured onto the plastic plates for growing bacterial colonies.

2.5.1.3 Ampicillin: 1mg ampicillin/mL .
2.5.1.4 Chloramphenicol: 12.5 µg chloramphenicol/mL.

2.5.1.5 SOB medium**:** Add the following in 490 mL of water.

10g Trypton from Casein
2.5g Yeast extract
0.25g NaCl
0.09g KCl

And autoclave at 121°C. SHP- Laboklav 25 was used to autoclave.
Add 5mL of 1M $MgSO_4$ and 5mL of 1M $MgCl_2$ to the autoclaved medium.
1M $MgSO_4$: 24.648g in 100mL water, filter sterilized.
1M $MgCl_2$: 20.33g in 100mL water, filter sterilized.

2.5.1.6 TB Buffer: Add the following chemicals in 100mL water.

220.5 mg $CaCl_2$ (15mM)
1.864g KCl (250mM)
0.30237g PIPES (10mM)
0.9895g $MnCl_2$ (50mM)

And the pH is adjusted with 1N KOH to 6.75 and the solution is then filter sterilized.

2.5.2 For immunohistochemistry:

2.5.1.7 Gelatin Albumin Mixture:
24.2g albumin is dissolved to 66mL H_2O at R.T. with continuous stirring to avoid formation of clumps.

5.7g gelatin is dissolved to 25mL H_2O pre-heated to about 55°C in a water-bath. Gelatin is added in small amounts each time to water to avoid formation of clumps.
The gelatin solution is then added to albumin solution with continuous stirring.

2.5.1.8 4% PFA: 4g of paraformaldehyde is added to 100mL H_2O.

2.5.1.9 6% PFA: 6g of paraformaldehyde is added to 100mL H_2O.

2.5.1.10 10X PBS: Add the following chemicals in 1000mL water.

8.5g NaCl

1.5g Na_2HPO_4. $2H_2O$

0.21g NaH_2PO_4. H_2O

Adjust the pH to 7.4.

2.5.1.11 1% PBT: Add 1mL Triton-X to 100mL 1X PBS.

2.5.1.12 Blocking solution: 0.25g Bovine serum albumin (BSA) and 1mL of Normal goat serum (NGS) dissolved in 10mL 1% PBT.

2.6 List of chemicals:

Chemical	**Company**	**Catalog no.**
Agarose	Applichem	A21114.0500
Albumin	Sigma	A5253
Ampicillin	Roche	835242
Bovine serum albumin	Applichem	A1391
Calcium chloride dihydrate ($CaCl_2$. $2H_2O$)	Applichem	10035-04-8
Chloramphenicol	Sigma	C0378
Cornmeal	Obermühle Rosdorf	
DABCO	Roth	0718
Disodium phosphate (Na_2HPO_4)	BioChemica	A3905,0500
Ethanol	J.T.Baker	8006
Gelatin	Sigma	G2500
Glycerol	Th.Geyer Chem$^{solute®}$	2039,1000
Hydrochloric acid (HCl)	Applichem	A6578,0500
Isopropanol	AppliChem	A3928,0500GL
Luria agar	Sigma	L2897
Luria broth (LB)	Sigma	L3022

Malzin	Ulmer Spatz	
Magnesium chloride ($MgCl_2$)	Merck	2170690
Magnesium sulphate ($MgSO_4$)	Merck	1.05886
Manganese chloride ($MnCl_2$)	Merck	A475734
Methanol	Roth	8388
Nipagin	Sigma-Aldrich	54750
Normal goat serum	Jackson Immuno	005-000-121
Paraformaldehyde (PFA)	Merck	104051000
PIPES	Applichem	A1079
Propionic acid	Merck	8006050100
Potassium chloride (KCl)	Apllichem	7447-40-7
Potassium hydroxide (KOH)	Applichem	A3871
Sodium chloride (NaCl)	AppliChem	A2942.1000
Sodium dihydrogen phosphate monohydrate (NaH_2PO_4. H_2O)	BioChemica	A1047.0500
Sodium hydroxide (NaOH)	AppliChem	A6829.0500
Treacle	Hellmi	1905
Tris base	AppliChem	A2264.1000
Triton-X	AppliChem	A1388.0500
Trypton	Roth	8952.2
Yeast extract	Roth	2363.2

2.7 List of molecular biology reagents:

Reagent	**Company/ Source**	**Catalog no.**
dATP	Invitrogen	55082
dTTP	Invitrogen	55085
dGTP	Invitrogen	55084
dCTG	Invitrogen	55083
BioThermPlus Taq DNA polymerase	Genecraft	GC-061-0250
Phusion for high fidelity PCR	ThermoScientific	F-553S
GeneRuler DNA ladder mix	ThermoScientific	SM0321
Roti-safe gelstain	Carl Roth	3865.1

Rapid DNA Dephos & DNA ligation kit	Roche	04 898 117 001
TOPO TA cloning kit	Invitrogen	450641
QIAquick DNA purification kit	Qiagen	28104
QIAquick Gel Extraction kit	Qiagen	28704
Invisorb®Spin Plasmid Mini Two	Invitek	1010140400
GenElute™ Plasmid Midiprep Kit	Sigma Aldrich	PLD35
XL-1 Blue Competent Cells	Stratagene	200 236
ZR Tissue and Insect RNA Microprep kit	ZymoResearch	R1060
Quantitect Reverse Transcription kit	Qiagen	205311
FastDigest EcoR1	Fermentas	FD0274
FastDigest BamH1	Fermentas	FD0054
FastDigest Xba1	Fermentas	FD0684
FastDigest Eag1	Fermentas	FD0334
FastDigest Ase1	Fermentas	FD0914
Blood and tissue kit	Qiagen	69504

2.8 List of antibodies:

Antibody	**Source**	**Catalog no.**	**Dilution used**
Rabbit anti-HRP	Invitrogen	G21234	1:1000
Mouse anti-Futsch/ 22c10	DSHB		1:500
Rabbit anti-GFP polyclonal	Abcam	ab6556	1:1000
Mouse anti-NOMPC	Prof. Joe Howard, MPI CBG, Dresden		1:1000
Rat anti-IAV	Prof. Changsoo Kim, Chonnam University, Seoul		1:1000
Alexa Fluor 647 phalloidin	Invitrogen	A22287	1:50
Alexa Fluor goat anti-rabbit 488	Invitrogen	A11008	1:300

Alexa Fluor goat anti-rabbit 633	Invitrogen	A21070	1:300
Alexa Fluor goat anti-mouse 488	Invitrogen	A21042	1:300
Alexa Fluor goat anti-mouse 546	Invitrogen	A11030	1:300
Alexa Fluor goat anti-rat 633	Invitrogen	A21094	1:300

2.9 List of flies used:

Genotype	**Source**
Canton S	Bloomington
w^{1118}	Frank Sprenger
y, w; Sp/ CyO; MKRSb/ TM6Tb	Hugo Stocker
Sm6a-Trans(MiT)hs24/ noc (sco)	Bloomington
w^{1118}; Mi{ET1}CG17150^{MB05004}/TM6C, Sb1 (BL24844)	Bloomington
y^{1} w^{*}; Mi{MIC}CG17150^{MI00310}/TM6B, Tb^{1} (BL30957)	Bloomington
w^{1118}; Mi{ET1}CG6053^{MB06262} (BL25491)	Bloomington
w^{1118}; Mi{ET1}CG9313^{MB06913}	Bloomington
w^{1118}; Mi{ET1}Dhc62B^{MB12102}	Bloomington
w^{1118}; Mi{ET1}Dhc93AB^{MB04366}	Bloomington
iav^{1}/ FM7c	Bloomington
nan36a	Bloomington
nan^{dy5}/ TM6Tb	Bloomington
w^{1118}; Mi{ET1}CG17150^{MB05004}-nan^{dy5}/ TM6C, Sb	Prof. Maurice Kernan, SUNY
F-Gal4	Prof. Changsoo Kim, Chonnam University, Seoul
CG6053 Gal4 (dmdnai2 Gal4)	Self-generated
CG17150 Gal4 (dmdnah3 Gal4)	Dr. Daniel Eberl, University of Iowa
UAS CG6053 (UAS dmdnai2)	Self-generated
UAS CG6053-YFP (UAS dmnai2-YFP)	Self-generated
pBAC70G22/ CyO (dmdnai2 genomic rescue*)*	Self-generated

CG17150 MSSMR WT #67-1 + CG17150[Minos-MB05004] recomb. F/TM3, Sb (*dmdnah3* genomic rescue in *dmdnah3* mutant background)	Dr. Daniel Eberl, University of Iowa
UAS GFP-T2	Bloomington

The names in the brackets indicate the name with which these fly lines are referred to later in the thesis.

3. Results.

3.1 Possible roles of axonemal dyneins in the fly auditory system.

3.1.1 Mutant analysis.

Electron microscopic analyses suggest presence of dynein-like arms in the proximal region of the dendritic cilia of JO neurons, which spans from basal bodies to ciliary dilation along the length of dendrites. We identified several axonemal dyneins in *Drosophila melanogaster* based on sequence similarity with the known axonemal dynein proteins in humans. (Fig. 3.1) 11 axonemal dynein heavy chains, 2 axonemal dynein intermediate chains, 1 axonemal dynein light intermediate chain and 2 axonemal dynein light chains were identified. Using available mutants of 5 axonemal dynein heavy chain and 2 axonemal dynein intermediate chain auditory performances were analyzed by measuring sound-evoked antennal movements using laser Doppler vibrometry and sound-evoked compound action potentials from the antennal nerve (with David Piepenbrock).

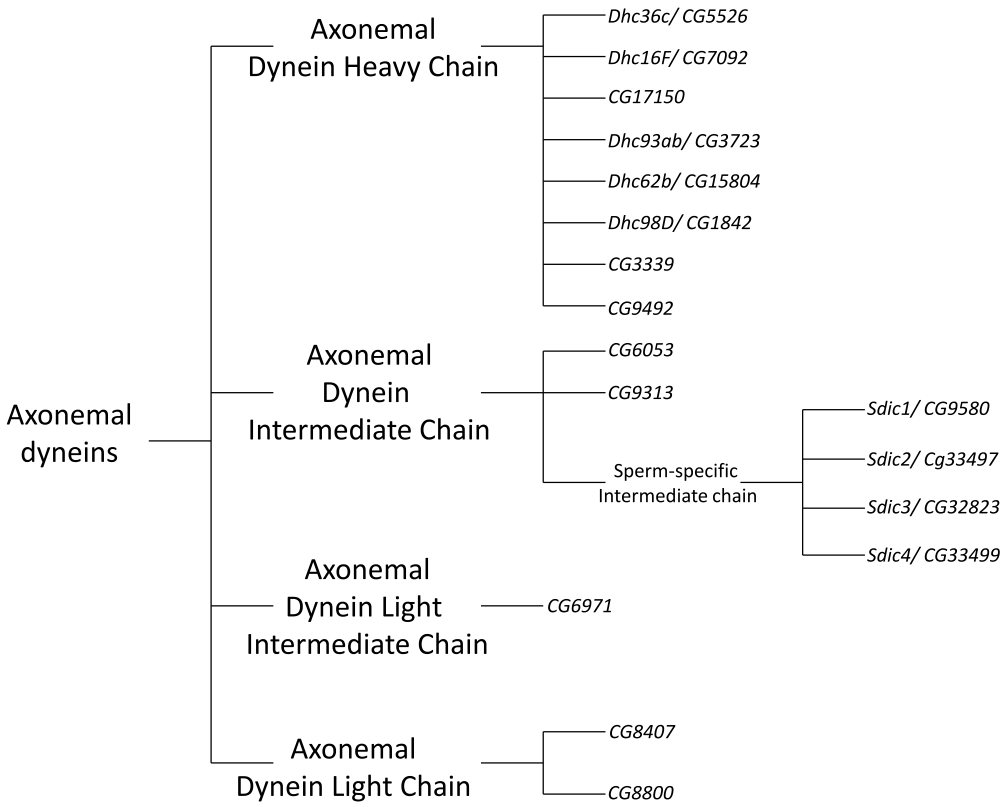

Fig. 3.1: A dendogram representing axonemal dynein family in *Drosophila melanogaster*. Axonemal dyneins are made up of heavy, intermediate, light intermediate and light chains. The known genes encoding for these chains in *Drosophila melanogaster* are listed here.

Fly antennae show fluctuations in absence of sound stimuli. These free mechanical fluctuations were monitored by the vibrometer to measure the velocity of the antennal movements over time. Fourier transformation of the velocity trace shows frequency tuning of antenna (Fig. 3.2). The frequency at which the velocity of an antenna is the highest is considered as the individual best frequency of each antenna. Respective antennal displacements and power spectrum of the system can also be deduced, providing hints about the activity of the system.

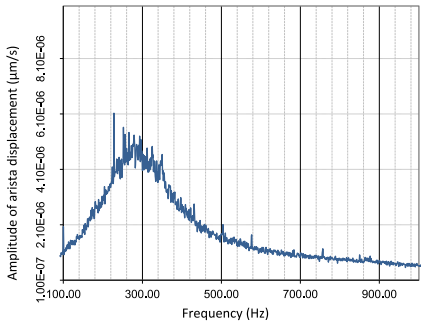

Fig. 3.2: Frequency tuning of wild-type antenna. A fast Fourier transform of velocity trace of wild-type antenna into frequency domain shows that the antenna is tuned at around 250-300 Hz.

Pure tone sine stimuli at intensities varying over 5 orders of magnitude at the antennal best frequency are presented to each individual fly. *Canton S* (*CS*) and *white* mutants (w^{1118}) are considered wild-type and genetic background controls respectively in our study. Antennae of wild-type flies show roughly 10-fold higher sensitivity (measured as antennal displacement with respect to sound particle velocity) at low intensity stimuli (sound particle velocity in the order of 10^{-3} mm/s) than at high intensity stimuli (sound particle velocity in the order of 10^{2}mm/s) (Fig. 3.3). Since flies can only detect near-field sounds, sound stimuli are converted into respective sound particle velocities in our measurements. A physiologically active antenna shows relatively lower best frequency of the antennal fluctuations, higher power spectrum and higher sensitivity gain as compared to a deaf fly which mimics a physiologically compromised state or a passive system (shown by the dotted line in Fig. 3.3a). The power gain in the system can be explained by gating spring model, which links the antennal mechanics to the activity of ion channels and adaptation motors in the system.

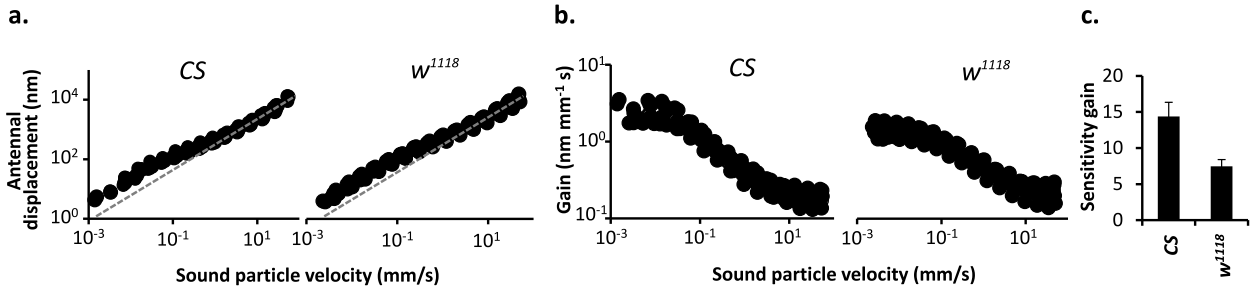

Fig. 3.3: Active antennal mechanics. a. Antennal displacements are plotted against the sound particle velocity that is a measure of sound intensity. The plot shows compressive nonlinearity as antennae show higher displacements towards lower sound intensities as compared to a passive system. The straight dotted line in grey shows linear behavior of a passive system. b and c. Gain is measured as a ratio of antennal displacement (output) by sound particle velocity (input). The antennae show about a 10-fold higher gain at low sound intensities than at high ones. Sensitivity gain is

calculated as a ratio between the highest gain and the lowest gain shown by an antenna when presented with sound intensities differing by 5 orders of magnitude. N≥5.

The sound-evoked nerve responses are measured as compound action potentials (CAP) from the antennal nerve. (Fig. 3.4)Tungsten electrodes are inserted in the head roughly near the antennal nerve to detect these signals. The exact position of the electrodes determines the absolute CAP amplitudes and hence a significant variability is observed generally in these measurements. In order to compare the CAP responses from different animals and be able to measure the threshold of antennal nerve firing it thus, becomes necessary to normalize the CAP response. The CAP amplitudes are normalized such that the maximum CAP response for each fly is taken as 1 and the least response as 0. Normalized CAP response when plotted against sound stimulus intensity or antennal displacement shows a sigmoidal curve that can be fitted with a Hill equation. Threshold of sound-evoked nerve response for each fly was determined by the sound particle velocity corresponding to 10% of the highest compound action potential shown by each fly. Sound intensities in the range of 0.04-0.05 mm/s and antennal movements in the range of about 50-100 nm mark the threshold of the sound-evoked antennal nerve responses in wild type flies. The antennal displacements corresponding to 10% and 90% of the maximum sound-evoked nerve response define the dynamic range. Shifts in threshold hint at increased stiffness of the system. While shift in dynamic range of antennal displacement to elicit a nerve response suggests that only a sub-population of JO neurons are affected and the remnant nerve response seen is due to firing of neurons that are activated in the higher antennal displacement regime, for example the wind and

gravity sensing CE-neurons.

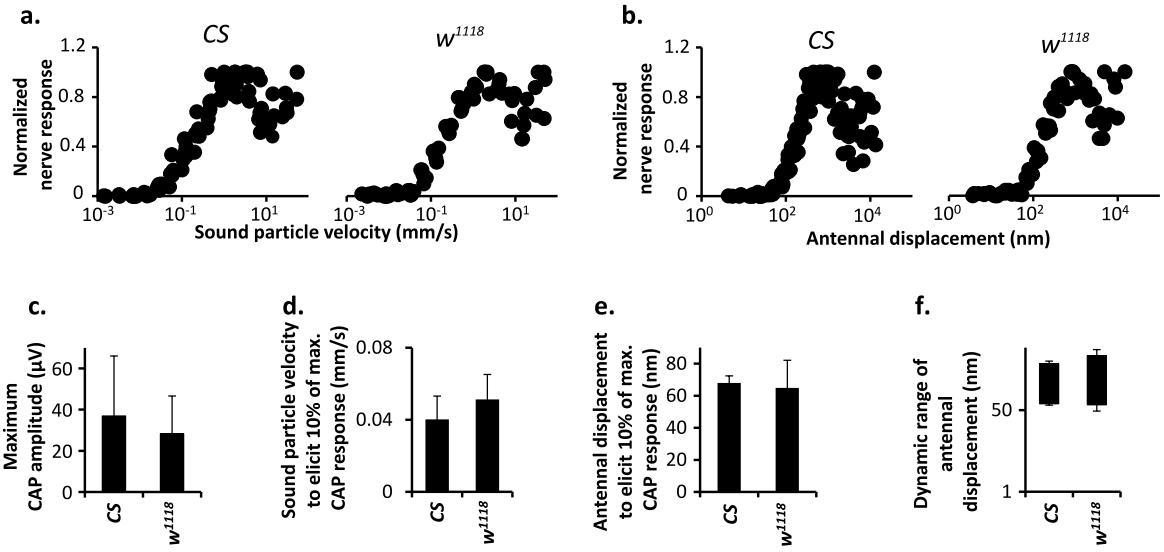

Fig. 3.4: Sound-evoked compound action potentials in JO neurons. a and b. CAP responses are plotted against sound stimuli of intensities varying by 5 orders of magnitude. The highest CAP response shown by an animal is set to 1 and the least to 0. Nerve response when plotted against sound particle velocity and antennal displacement shows a sigmoidal curve that can be fitted with a Hill equation. c. Maximum CAP amplitude. d and e. The Hill equation fit is used to calculate the threshold of antennal nerve towards sound and antennal displacement. f. Dynamic range of antennal displacement corresponding to CAP response is plotted as box plot. The displacements corresponding to 10% of the maximum CAP response is shown by the lower end of the box and the upper end denotes the displacements corresponding to 90% of the maximum CAP response. N≥5.

In *Drosophila melanogaster* motile axonemes have been reported only in sperms and chordotonal organ neurons so far. We checked mutants of various axonemal dynein proteins assuming that mutation in each of these proteins would affect the functioning of the dynein regulatory complex (forming the dynein arms) that they are a part of. All of the mutants contain a Minos insertion in the exon of the gene in a w^{1118} background. The phenotypes of the mutants studied are compiled in figures 3.5, 3.6 and 3.7. According to our analyses each axonemal dynein protein has a unique role as summarized in the table 1.

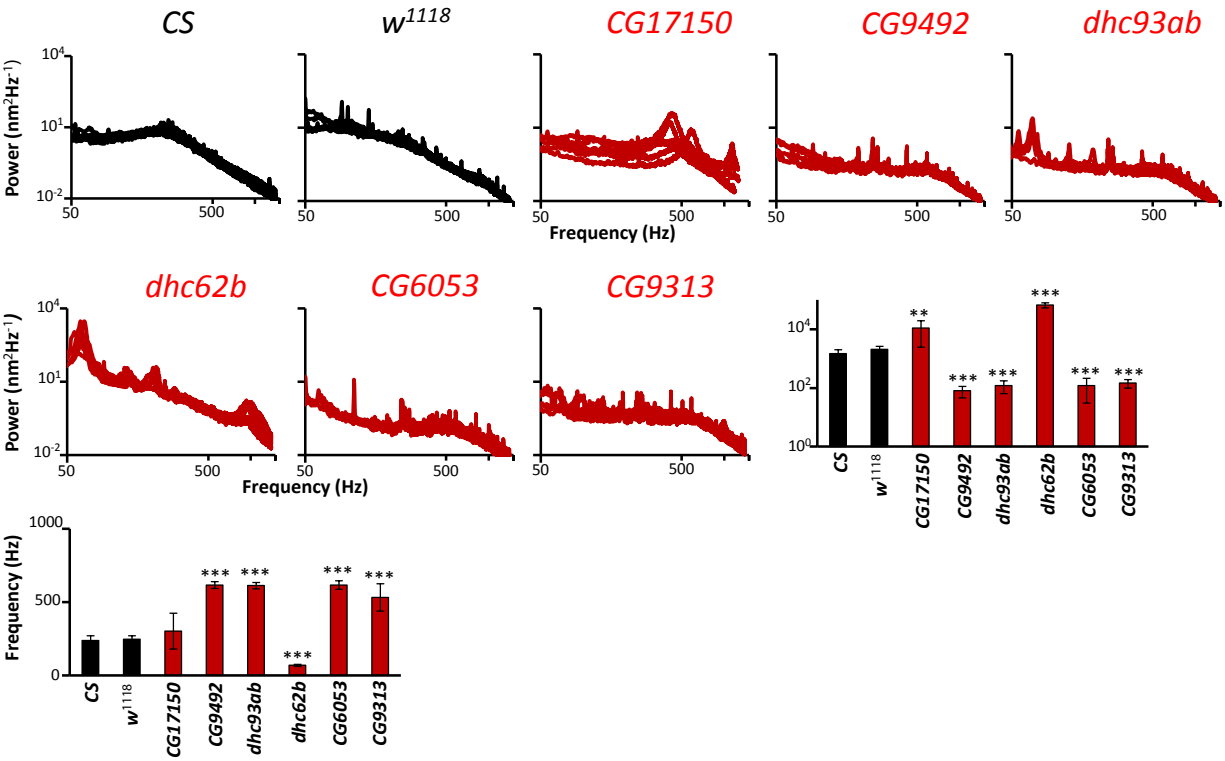

Fig. 3.5: Antennal fluctuations analysis of axonemal dynein mutants. a and b: Power spectra obtained for each genotype id obtained. Power is measured as the square of the antennal displacement divided by frequency. Total power (b) is calculated by summing the square of the antennal displacements between 50 to 1400 Hz. c. The best frequency of each genotype is measured from the Fourier transform trace of antennal velocity where the antenna shows the maximum velocity.

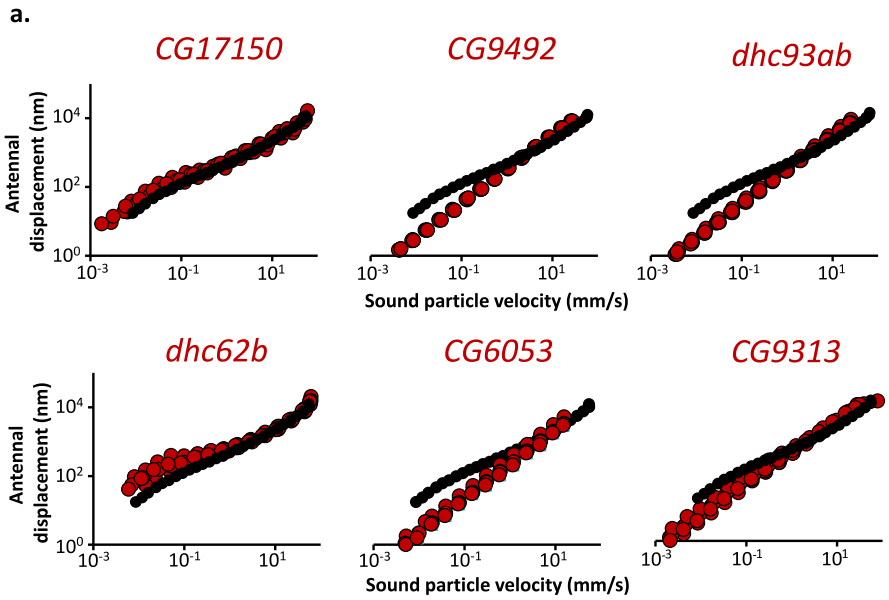

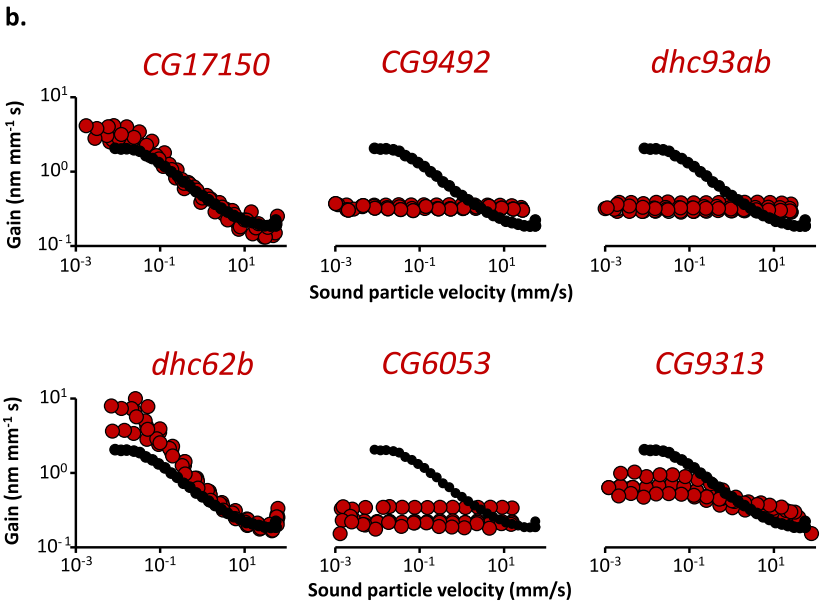

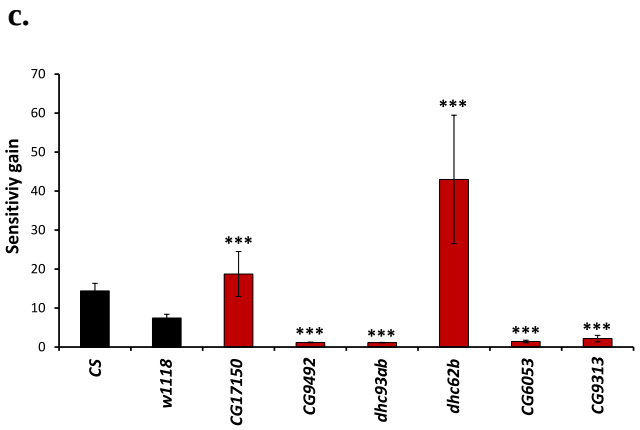

Fig. 3.6: Nonlinear compression and power gain in axonemal dynein mutants. a and b. Antennal displacements and gain respectively are plotted against the sound particle velocities for each genotype. The black dots show the wild-type flies response while red denotes the respective mutants. c. Nonlinear sensitivity gains of the mutants are compared with the wild-type flies. The black dots in a and b denote wild-type response. N≥4. *** denotes p<0.01 (Student's t-test).

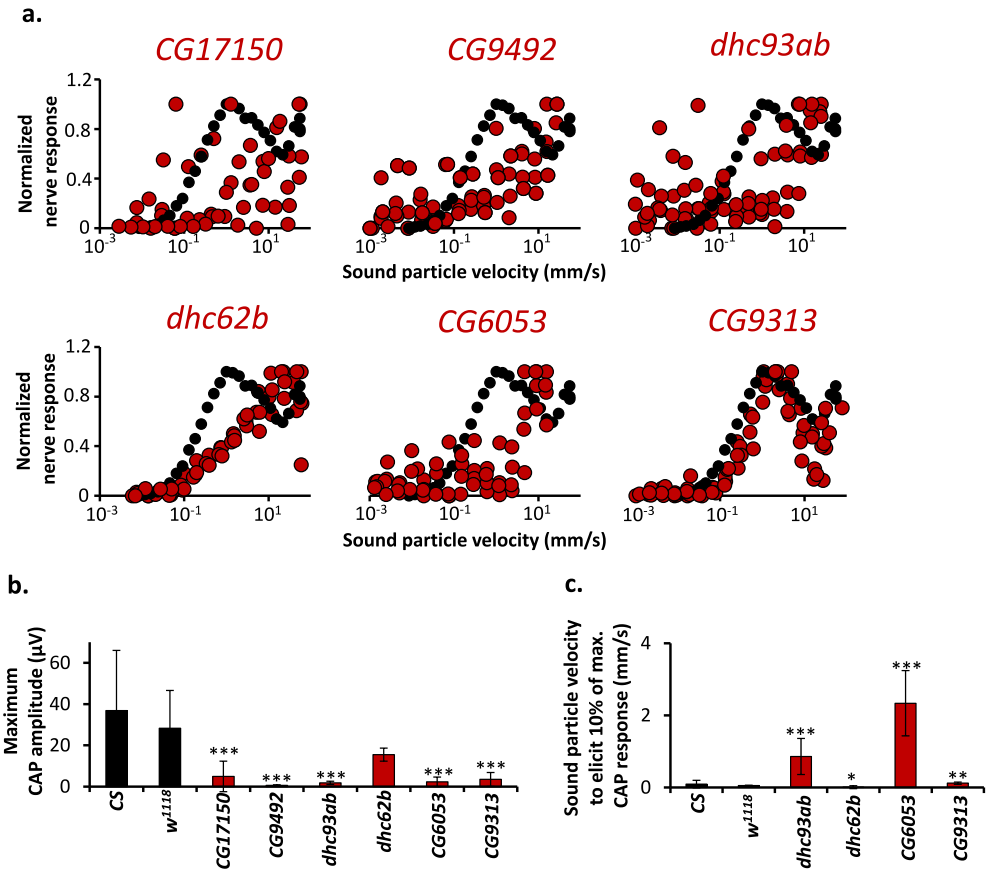
a.
CG17150
CG9492
dhc93ab
dhc62b
CG6053
CG9313
Normalized nerve response
Sound particle velocity (mm/s)
b.
Maximum CAP amplitude (µV)
c.
Sound particle velocity to elicit 10% of max. CAP response (mm/s)
CS
w1118
CG17150
CG9492
dhc93ab
dhc62b
CG6053
CG9313

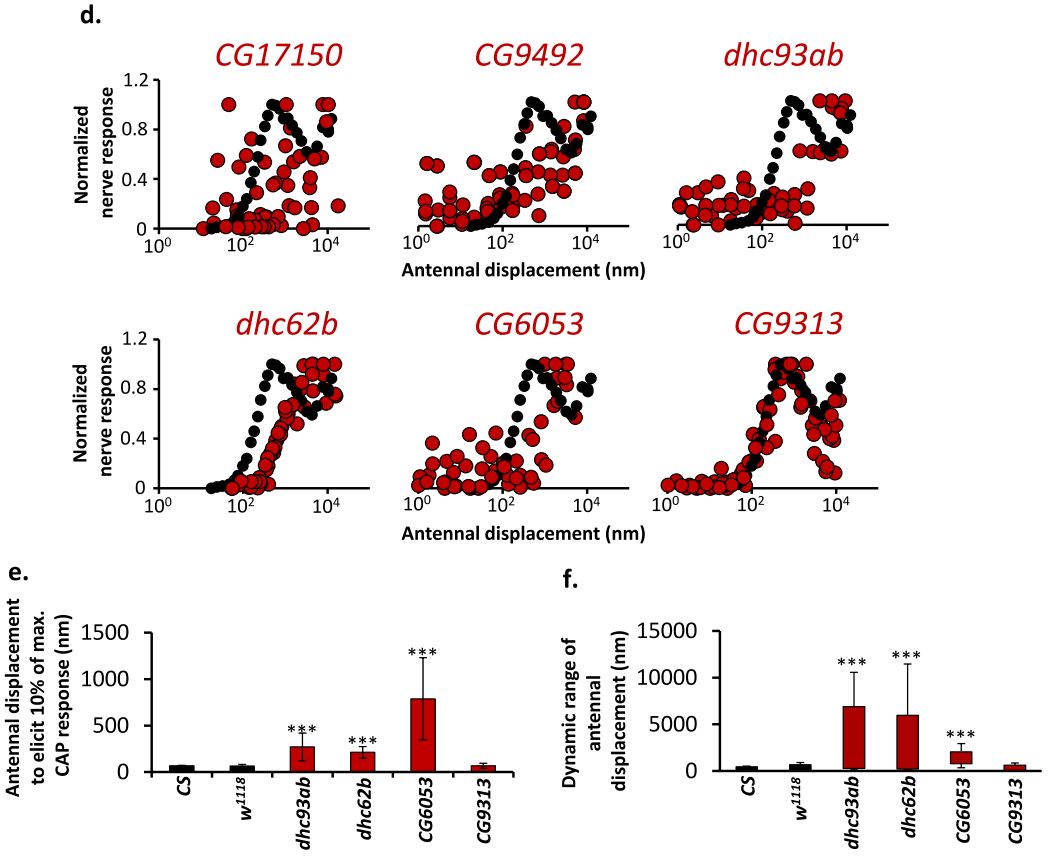

Fig. 3.7: Nerve responses in axonemal dynein mutants. a and c: Normalized nerve responses of mutants are plotted against the corresponding sound particle velocity and antennal displacements, respectively. b. Maximum CAP amplitudes for each genotype are plotted and compared with those of wild-type flies. c and e: Threshold of the antennal nerve to sound particle velocity and antennal displacement are measured by calculating the sound intensity and displacement corresponding to 10% of the maximum CAP response. f. Dynamic range of antennal displacements for each genotype are plotted as box plots. The lower end of the plots represent the antennal displacements corresponding to 10% of maximum CAP response and the upper end corresponds to the displacements at 90% of CAP response. The black dots in a and d denote wild-type response. N≥4. *** denotes $p<0.01$, **$p<0.05$, *$p<0.1$ (Student's t-test).

Table 1: Summary of changes in antennal mechanics and nerve responses in axonemal dynein mutants.

Gene	***Human homologue (by protein similarity)***	***Mutant phenotype***			
		Best frequency	***Power spectrum***	***Amplification***	***Nerve response***
CG17150	*DNAH3* (axonemal inner arm heavy chain)	Similar to WT	Slightly higher in younger flies	Intact, slightly higher in younger flies	Complete loss
CG9492	*DNAH5* (axonemal outer arm heavy chain)	Higher than WT	Reduced	Loss	Complete loss
Dhc93ab/	*DNAH17*	Higher	Reduced	Loss	Reduced

CG3723	(axonemal outer arm heavy chain)	than WT			amplitude with shift in displacement sensitivity
Dhc62b/ CG15804	*DNAH12* (axonemal inner arm heavy chain)	Lower than WT	Higher	Excess	Reduced amplitude with shift in displacement sensitivity
CG6053	*DNAI2* (axonemal outer arm intermediate chain)	Higher than WT	Reduced	Loss	Reduced amplitude with shift in displacement sensitivity
CG9313	*DNAI1* (axonemal inner and outer arm intermediate chain)	Higher than WT	Reduced	Loss	Reduced amplitude with a shift in stimulus intensity sensitivity

CG17150 mutant antennae have a comparable best frequency as the WT (w^{1118})flies but show slightly higher power spectra and amplification. Sound-evoked antennal nerve responses were lost in these mutants. The responses seen at double the frequency of stimulus were indistinguishable from noise for most of the intensities. At higher intensities the electrodes pick signal because of break-through. This suggests that mechanotransduction machinery is intact at the tip of the auditory neurons in these mutants. However, amplification/propagation of the signal along the length of the neurons might be affected explaining the loss of sound-evoked action potentials in the antennal nerve. *Dhc62b* mutant antennae show significantly lower best frequencies and higher power spectra. Amplification is higher and sound-evoked nerve responses are reduced. The remnant nerve response shows a shift in sensitivity towards antennal displacements. This hints that the response due to the neurons responsive to higher

displacements is still intact in these mutants. However, since these mutants show intact amplification both *CG17150* and *Dhc62b* might serve regulatory/ modulatory roles in the fly auditory system.

Mutation in *CG9492* causes shift of best frequency of the antennae towards the higher regime, results in reduced power spectra, loss of both active amplification and does not show sound-evoked antennal nerve response that can be distinguished from noise. This suggests the function of this gene is required in all JO neurons. *Dhc93ab* and *CG6053* mutants show higher antennal best frequency, reduced power spectra, loss of active amplification and reduction in sound-evoked antennal nerve response in the JO neurons. The remnant nerve response with a shift in sensitivity towards antennal displacement in *CG6053* mutants suggests that these genes function mainly in the fly auditory neurons. On the other hand mutation in *CG9313* causes loss of power in the system, loss of active amplification and reduction in antennal nerve response to sound stimuli. However, the remnant nerve response shows only a shift in sensitivity only towards sound stimuli intensities. The sensitivity of the JO neurons towards antennal displacement remains intact in these mutants. Thus, *CG9313* seems to function only in a population of JO neurons such that loss of its function increases stiffness of the system causing shift of sensitivity of the neurons towards sound stimuli. But functioning of some of the auditory neurons still remains unaffected so as to maintain the sensitivity of the neurons towards antennal displacement.

Thus, axonemal dyneins are not only required for active amplification and to endow the auditory system with higher sensitivity to lower intensity stimuli but some of them also serve modulatory roles (like *CG17150* and *Dhc62b*). In this thesis the details of the roles of *CG6053* and *CG17150* in fly auditory system will be further discussed.

3.1.2 Roles of dmDNAI2 in active amplification in Drosophila auditory system.

By sequence similarity *CG6053* is homologous to *DNAI2* (axonemal dynein intermediate chain 2) in humans. Mutation in *dnai2* in humans is known to cause primary ciliary dyskinesia and thus, strongly suggests a motile role of *dnai2* in humans. *CG6053* shows 47.8% protein identity and 55.9% DNA sequence identity with the human DNAI2.

CG6053 will thus, henceforth, be referred to as dm*dnai2* in this thesis. The homology of *CG6053* with *DNAI2* from other mammals based on protein sequence similarity is shown in the table below:

Table 2: Protein sequence comparison of *CG6053* with *DNAI2* (Axonemal dynein heavy chain 2) among different animals.

Organism	Gene	e-value	Query coverage (%)	% identity	
				With protein	With gene
Homo sapiens	*DNAI2*	0	96	47.8	55.9
Pan troglodytes	*DNAI2*	3.00E-172	96	47.6	55.9
Macaca mulatta	*DNAI2*	4.00E-167	91	49.2	56.5
Canis lupus familiaris	*DNAI2*	0	90	47.9	56.6
Bos Taurus	*DNAI2*	0	96	48.7	55.8
Mus musculus	*Dnaic2*	0	96	47.9	56.4
Rattus norvegicus	*Dnai2*	0	90	47	55.8
Gallus gallus	*DNAI2*	0	97	48.4	55.9
Anopheles gambie	*AgaP_AGAP011539*	0	91	68.4	67.1

We obtained a fly stock (BL25491) with a Minos insertion located 1518 bps downstream the transcription start site of dm*dnai2* gene. When the mRNA expression of *dmdnai2* was checked by reverse transcription it was found that the dm*dnai2* homozygous mutants did not show any band corresponding to the transcript region checked.(Fig. 3.8) Thus, it confirmed that the Minos insertion in dm*dnai2* disrupts the gene transcription and thus, protein expression completely producing a null mutant.

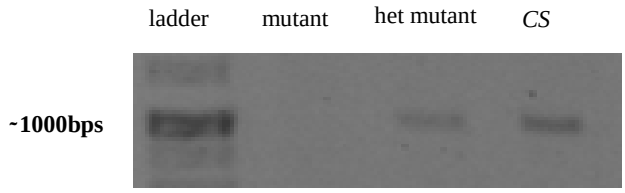

Fig. 3.8: RT-PCR analysis of dm*dnai2* mutants. mRNA expression of dm*dnai2* gene was checked in dm*dnai2* homozygous mutants, heterozygous mutants and wild-type (*CS*) controls by performing PCR on cDNA from each genotype.

The Minos insertion mutant of dm*dnai2* completely abolishes active amplification in the JO neurons and reduces the power spectra of the system and sound-evoked compound action potentials in the JO neurons drastically.(Fig. 3.9) The gain of the system reduces to 1.4 as compared to a gain of about 10 in wild type flies. Though most of the sound-

evoked nerve response is lost in the mutants there is a remnant nerve response with a significant shift in the sensitivity thresholds towards sound stimulus intensity (about 50 fold) and accordingly towards antennal displacement (Fig. 3.10). This suggests the responses arise from wind and gravity sensing neurons which are active in the higher antennal displacement regimes. The *dmdnai2* mutant phenotypes closely resemble the *NompC* mutants suggesting that there might be a link in the functioning of dm*dnai2* and *NompC*.

The phenotypes are rescued when the Minos insertion is precisely excised out by transposase activity introduced genetically and the gene functioned is regained. The genomic DNA of the excision line was sequenced to confirm the absence of Minos insertion in the dm*dnai2* coding region. This confirms that the phenotype seen was due to disruption in gene expression due to Minos insertion.

Genetic rescues by introducing the wild type copy of dm*dnai2* gene in the mutant background rescues the mutant phenotypes. The genetic rescues were performed in two ways: 1. By introducing a BAC clone of around 20kb carrying the wild type copies of dm*dnai2* and other genes flanking it. 2. By expressing the dm*dnai2* cDNA under the *UAS* promoter driven by *F-Gal4* specific for chordotonal organ neurons. Reversion of the mutant phenotypes by expression of the dm*dnai2* transcript shows that it was the disruption of dm*dnai2* gene function that caused loss of active amplification and sound-evoked nerve response in the mutant flies.

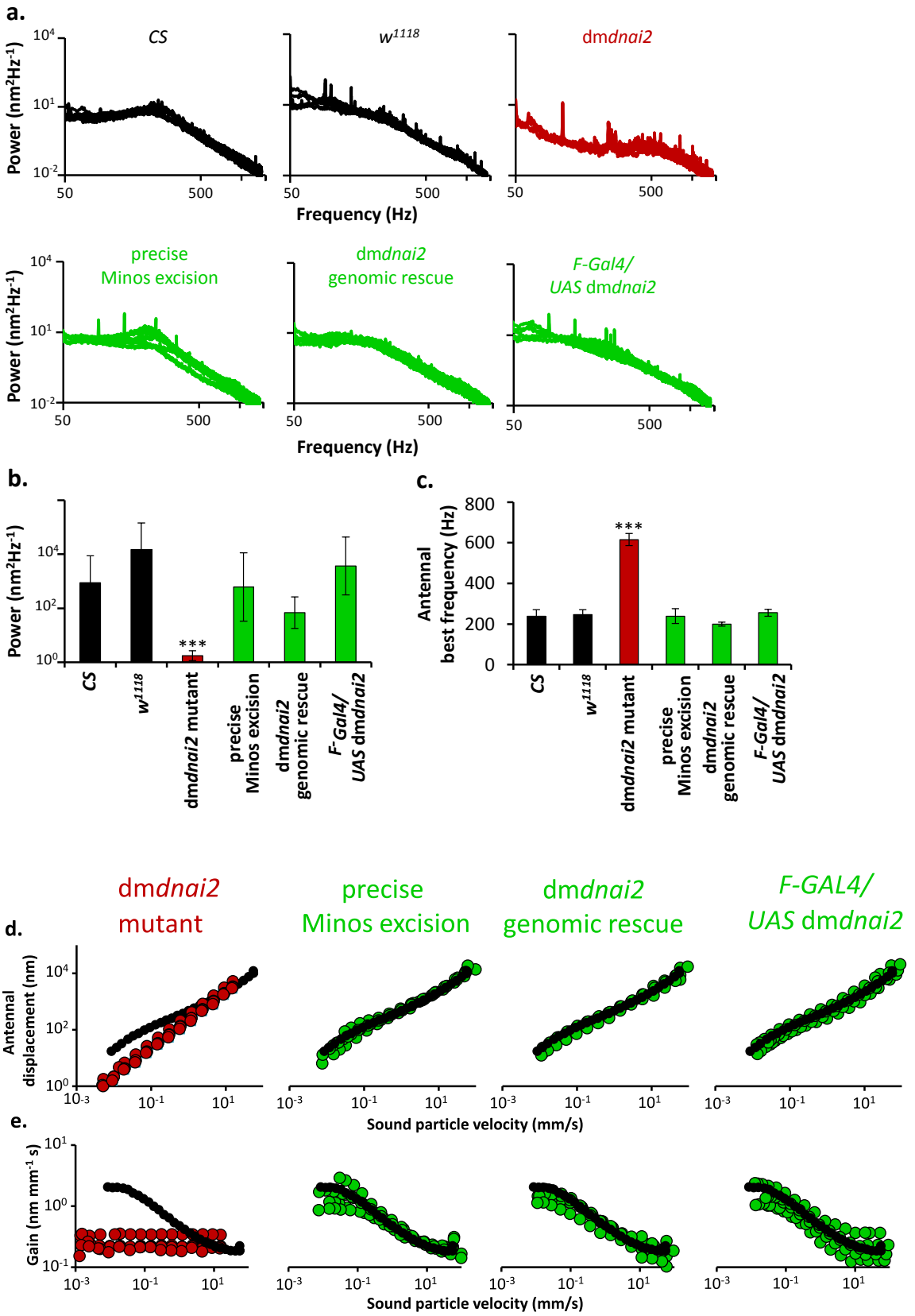
a.
CS
w1118
dmdnai2
Power (nm²Hz⁻¹)
Frequency (Hz)
precise Minos excision
dmdnai2 genomic rescue
F-Gal4/ UAS dmdnai2
b.
c.
Antennal best frequency (Hz)
***
dmdnai2 mutant
d.
Antennal displacement (nm)
Sound particle velocity (mm/s)
e.
Gain (nm mm⁻¹ s)

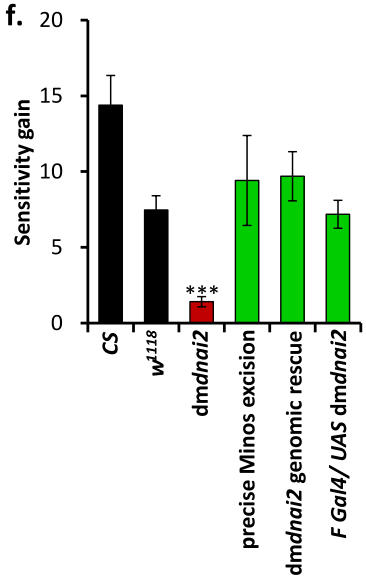

Fig. 3.9: Biomechanical analyses of dm*dnai2* mutants and genetic rescue control animals. a and b. The power spectra of animals of the respective genotypes are plotted and compared with the wild-type flies and the respective genetic rescue controls. c. The best frequency is plotted for each genotype measured. d and e. Antennal displacements and sensitivity gain for each genotype are plotted respectively against sound particle velocity. f. Sensitivity gain for each genotype is plotted to quantify power gain in the system. The black dots in d and e denote wild-type response. N≥4. *** denotes p<0.01 (Student's t-test).

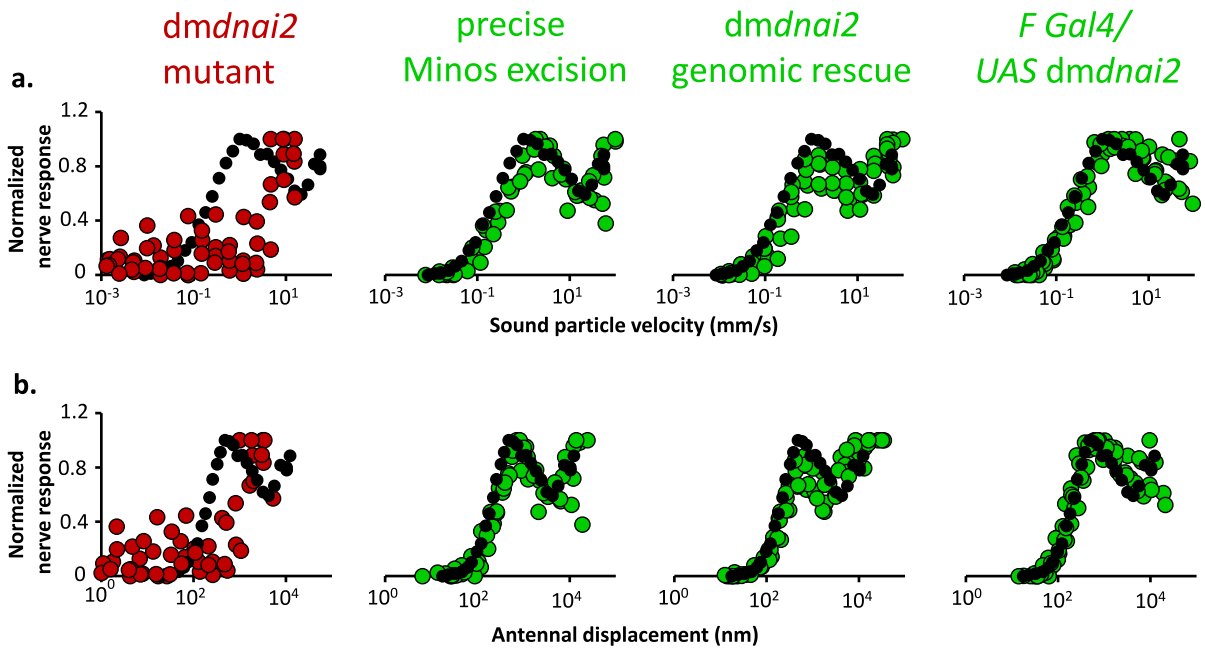

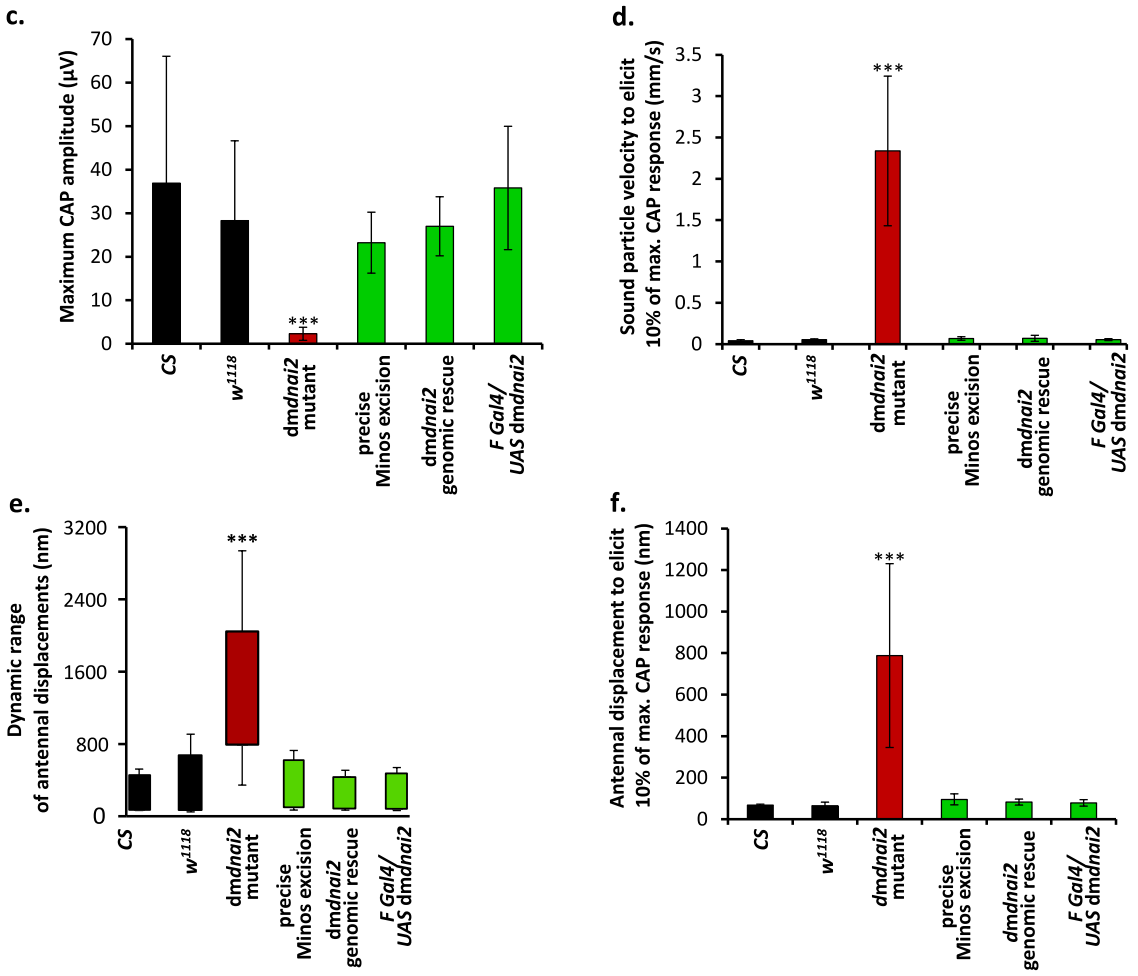

Fig. 3.10: Sound-evoked antennal nerve response analysis in dm*dnai2* mutants. a and b. Normalized nerve responses of dm*dnai2* mutants and the various controls are plotted against sound particle velocity and antennal displacements respectively. c. Maximum CAP amplitudes seen in each genotype are plotted. d and f. Antennal nerve threshold towards sound particle velocity and antennal displacement are plotted respectively by measuring the sound intensity and antennal displacement corresponding to 10% of maximum CAP response seen for each animal of each genotype. e. Dynamic range of antennal displacements eliciting sound-evoked nerve response is plotted for each genotype. The black dots in a and b denote wild-type response. N≥4. *** denotes $p<0.01$ (Student's t-test).

It was checked if the phenotypes seen in dm*dnai2* mutants are due to morphological or protein transport defects. The gross morphology of JO in the mutants was checked by staining the neurons with the neuronal marker horseradish peroxidase (HRP) and by using phalloidin to stain the actin-rich scolopale cells (Fig. 3.11a). The overall morphology of JO in the mutants seems comparable with the wild type flies. The expressions of the known mechanotransducing ion channels in the fly auditory system, TRPN1 (No Mechanotransducing Potential C, NOMPC) and a sub-unit of the modulatory TRPV channel (Inactive, IAV) were checked by staining with the respective antibodies.

IAV expression seems comparable with the wild type while NOMPC expression seems mislocalized. Not only in the distal parts like in the wild-type flies, dm*dnai2* mutants show expression of NOMPC even in parts of proximal region of the outer dendritic segment of JO neurons (shown with white arrow in Fig. 3.11b), overlapping significantly with the IAV expression, which can be seen evidently in the overlay panel of fig. 3.11b.
Since NOMPC is still expressed in dm*dnai2* mutants loss of amplification might occur in these mutants due to non-functionality of NOMPC channels. This hints at the requirement of axonemal dyneins to activate NOMPC channels to betray the active antennal mechanics. However, this result also hints at the role of axonemal dyneins in regulating NOMPC localization specifically. Since IAV expression and localization seem normal it can be said that axonemal dyneins do not have a common role in regulating localization of ciliary proteins.

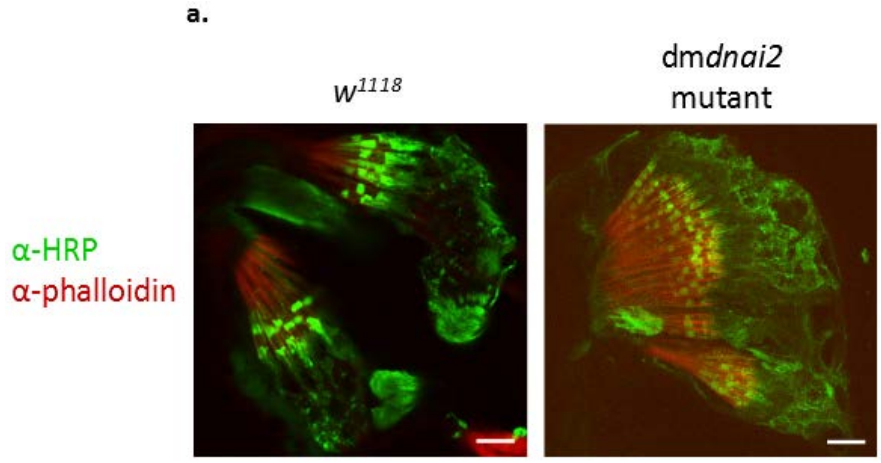

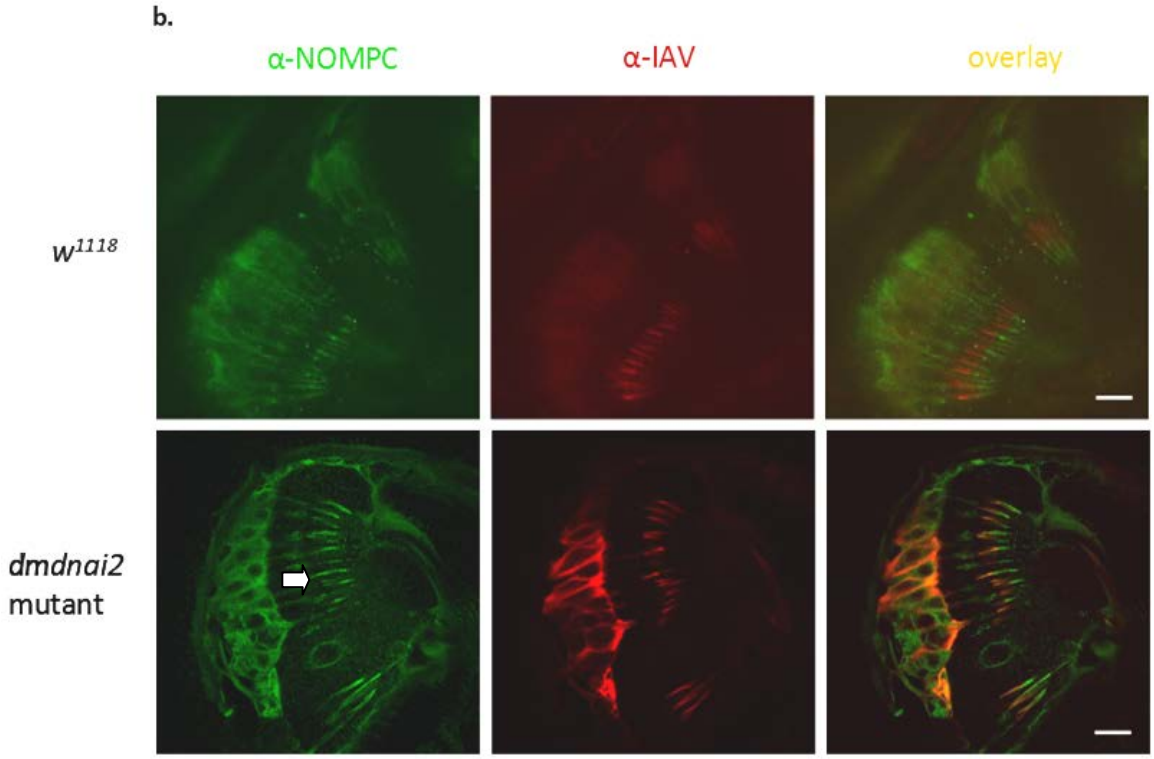

Fig. 3.11: Gross neuronal morphology and expression TRP channels in the JO neurons of dm*dnai2* mutants. a. The JO neurons of w^{1118} and dm*dnai2* mutant flies are stained with HRP (shown in green) and the scolopale cells with phalloidin (shown in red). b. Antibody staining against NOMPC and IAV are shown in green and red respectively in w^{1118} and dm*dnai2* mutants. Mislocalization of NOMPC in dm*dnai2* mutants is shown by white arrow. Scale bar: 10 µm.

3.1.3 Roles of dmDNAH3 in generation of sound-evoked Compound Action Potential in antennal nerve.

According to sequence similarity *CG17150* is the fly homologue of the human *DNAH3* (axonemal dynein heavy chain 3). It shows 50.3% protein sequence identity and 55.2% DNA sequence identity with the human DNAH3 protein. Thus, this gene will be referred to as *dmdnah3* in the thesis henceforth. The homology of *CG17150* with *DNAH3* from other mammals based on protein sequence similarity is shown in the table as follows:

Table 3: Protein sequence comparison of *CG17150* with *DNAH3* (axonemal dynein heavy chain 2) among different animals.

Organism	Gene	e-value	Query coverage (%)	% identity	
				With protein	With gene
Homo sapiens	*DNAH3*	0	86	50.3	55.2
Pan troglodytes	*DNAH3*	0	86	50.3	55.1
Macaca mulatta	*LOC697227*	0	89	49.5	54.4
Canis lupus	*DNAH3*	0	89	50.6	55

familiaris					
Mus musculus	*Dnahc3*	0	90	49.7	54.9
Rattus norvegicus	*Dnah3*	0	51	51.6	55.4
Gallus gallus	*DNAH3*	0	90	50.1	53.9
Danio rerio	*dnah3*	0	89	48	55
Anopheles gambie	*AgaP_AGAP002009*	0	94	61.1	62.8

We obtained a fly stock (BL24844) with a Minos insertion in its genomic DNA, at 3899 bps downstream the transcription start site of dm*dnah3*. The location of the Minos in the fly line was confirmed by performing polymerase chain reaction using genomic DNA (Fig. 3.12).

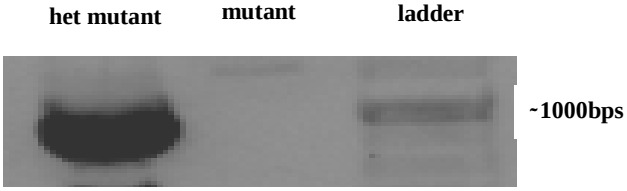

Fig. 3.12: Genomic DNA analysis of dm*dnah3* mutant. The position of the Minos insertion in the dm*dnah3* mutant (stock no. BL28444) was confirmed by performing PCR and comparing with the heterozygous mutants as positive control.

The Minos insertion causes a complete loss of sound-evoked antennal nerve response but does not affect active amplification or the power spectra of the auditory system (Fig. 3.13). When young (1-2 days old) the sensitivity gain shown by these flies is rather slightly higher than wild-type (Fig. 14). The age-dependence of this phenotype slightly resembles the *TrpV* (*nan-iav*) mutants though the difference in power and amplification in young and older *TrpV* mutants is significantly more drastic. While the older dm*dnah3* mutants resemble the wild-type flies the older *TrpV* mutants eventually turn completely deaf and behave like a passive system (data not shown). But this might still weakly hint towards a commonality in the mechanistic pathways of *dmdnah3* and *TrpV*.

It is interesting to note that mutation in dm*dnah3* renders a prominent but smaller peak in the higher frequency regime (~ 800-1000Hz) in addition to one seen at around 300Hz (Fig. 3.13a). Thus, mutation in this gene affects frequency tuning of the JO. But the mutants do not show any active amplification at this frequency regime.

When the Minos insertion is precisely excised out genetically by transposase activity the flies regain back the antennal nerve response to sound stimuli. (Fig. 3.13) Thus, the phenotype seen was due to the Minos insertion in the genome. Genetic rescues performed by introducing the wild-type copy of dm*dnah3* in the mutant background reverts back the

mutant phenotype.(Fig. 3.13) The plasmid used to insert the wild-type copy of dm*dnah3* contains a copy of the *white* gene. Thus, it makes *CS* (with the *white* gene) a better background control than w^{1118} for comparing the responses seen in these flies. The sound-evoked antennal nerve response in the genetic rescue line is comparable to the wild-type flies proving that the loss of sound-evoked antennal nerve response in the Minos insertion line is due to disruption of dm*dnah3* gene function.

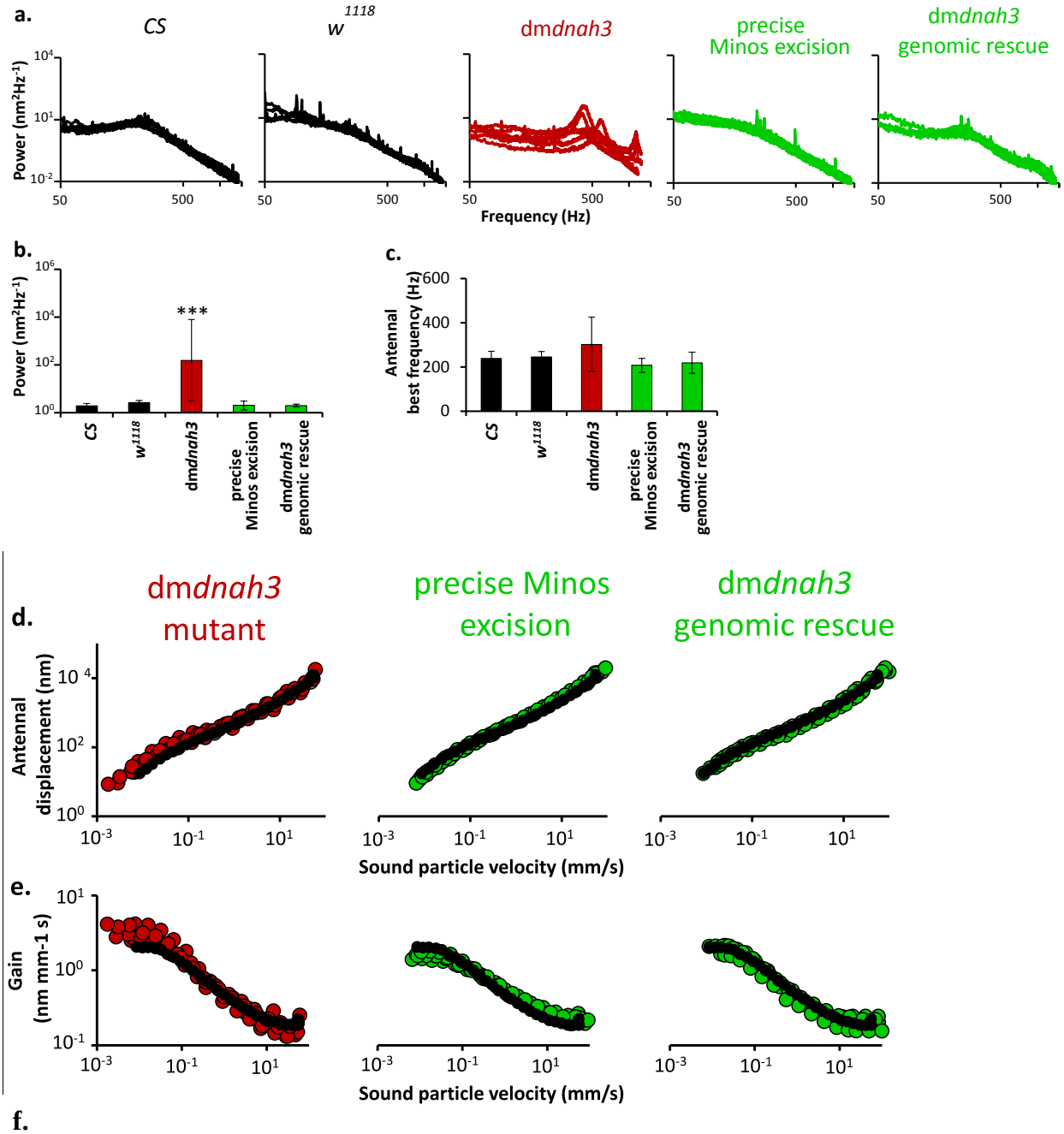

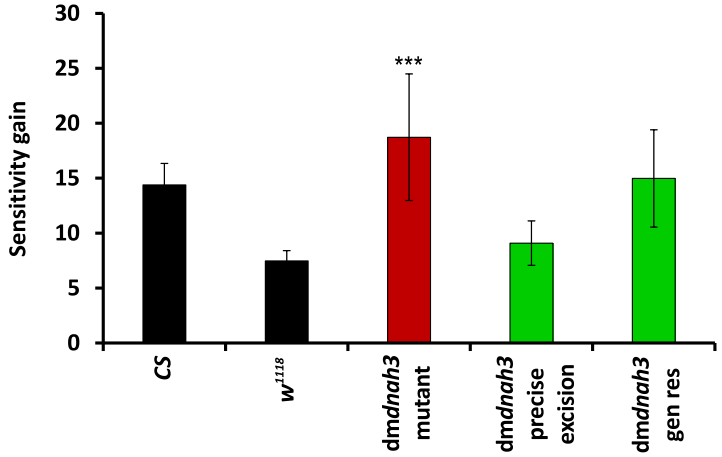
Sensitivity gain
30
25
20
15
10
5
0
***
CS
w1118
dmdnah3 mutant
dmdnah3 precise excision
dmdnah3 gen res

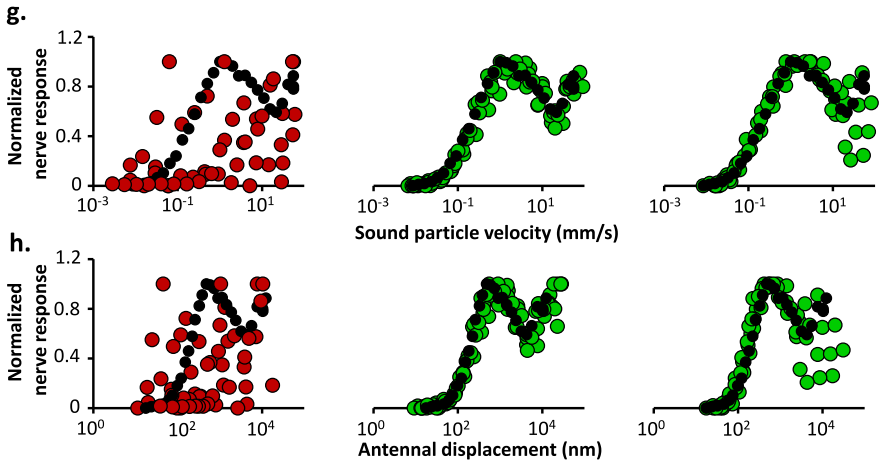
g.
Normalized nerve response
1.2
0.8
0.4
0
10-3
10-1
101
Sound particle velocity (mm/s)
h.
Normalized nerve response
1.2
0.8
0.4
0
100
102
104
Antennal displacement (nm)

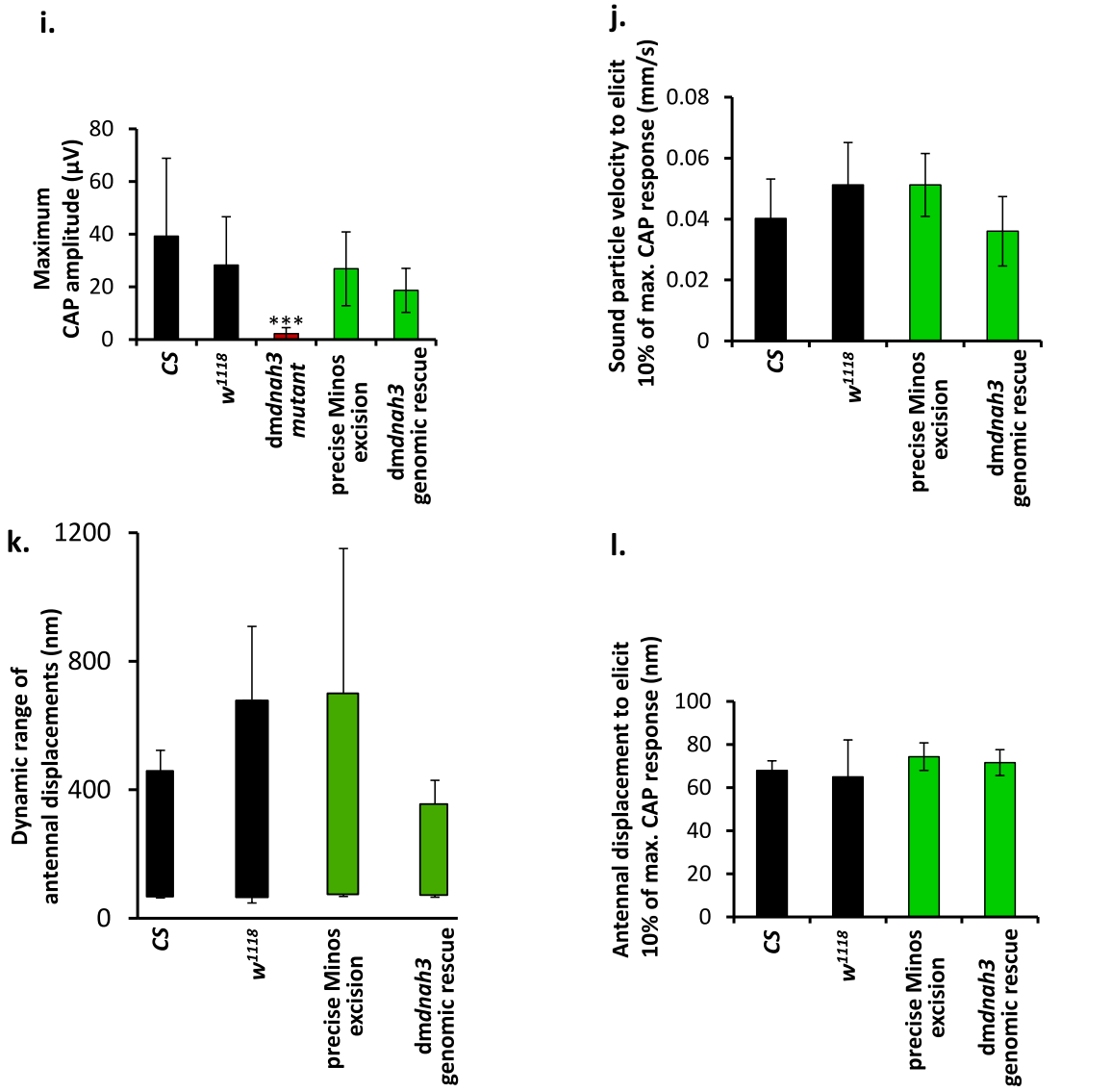

Fig. 3.13: Biomechanical and sound-evoked nerve response analyses of dm*dnah3* mutants and genetic rescue control animals. a and b. The power spectra of animals of the respective genotypes are plotted and compared with the wild-type flies and the respective genetic rescue controls. c. The best frequency is plotted for each genotype measured. d and e. Antennal displacements and sensitivity gain for each genotype are plotted respectively against sound particle velocity. f. Sensitivity gain for each genotype is plotted to quantify power gain in the system. g and h. Normalized nerve responses of dm*dnah3* mutants and the various controls are plotted against sound particle velocity and antennal displacements respectively. i. Maximum CAP amplitudes seen in each genotype are plotted. j and l. Antennal nerve threshold towards sound particle velocity and antennal displacement are plotted respectively by measuring the sound intensity and antennal displacement corresponding to 10% of maximum CAP response seen for each animal of each genotype. k. Dynamic range of antennal displacements eliciting sound-evoked nerve response is plotted for each genotype. The black dots in c, d, g and h denote wild-type response. N≥4. *** denotes $p<0.01$ (Student's t-test).

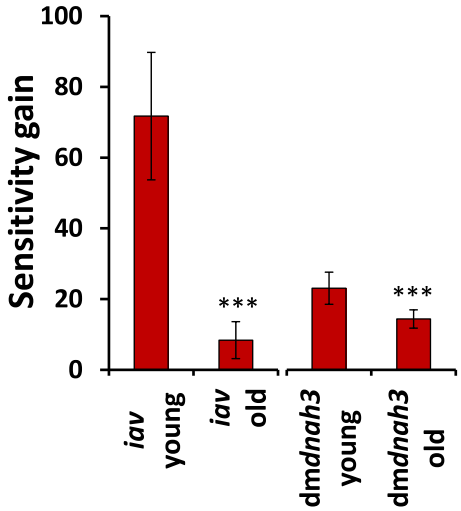

Fig. 3.14: Age-dependent power gain in TRPV and dm*dnah3* mutants. The young iav and dm*dnah3* mutants (1-2 days old) show significantly higher sensitivity gain than the older flies (more than 3 days old). N≥4. *** denotes p<0.01 (Student's t-test).

We obtained another Minos insertion mutant of dm*dnah3* gene (BL30957) which has the Minos insertion 4171 bps downstream the transcription site of dm*dnah3* gene in the genomic DNA. Though the Minos insertion in this case is in the intronic region it is only 272 bps downstream the insertion in stock BL 24844 and might affect an exon-intron splice junction. It shows the same auditory phenotype as the BL24844 line. It shows slightly intact amplification and does not show sound-evoked action potentials. (Fig. 3.15).

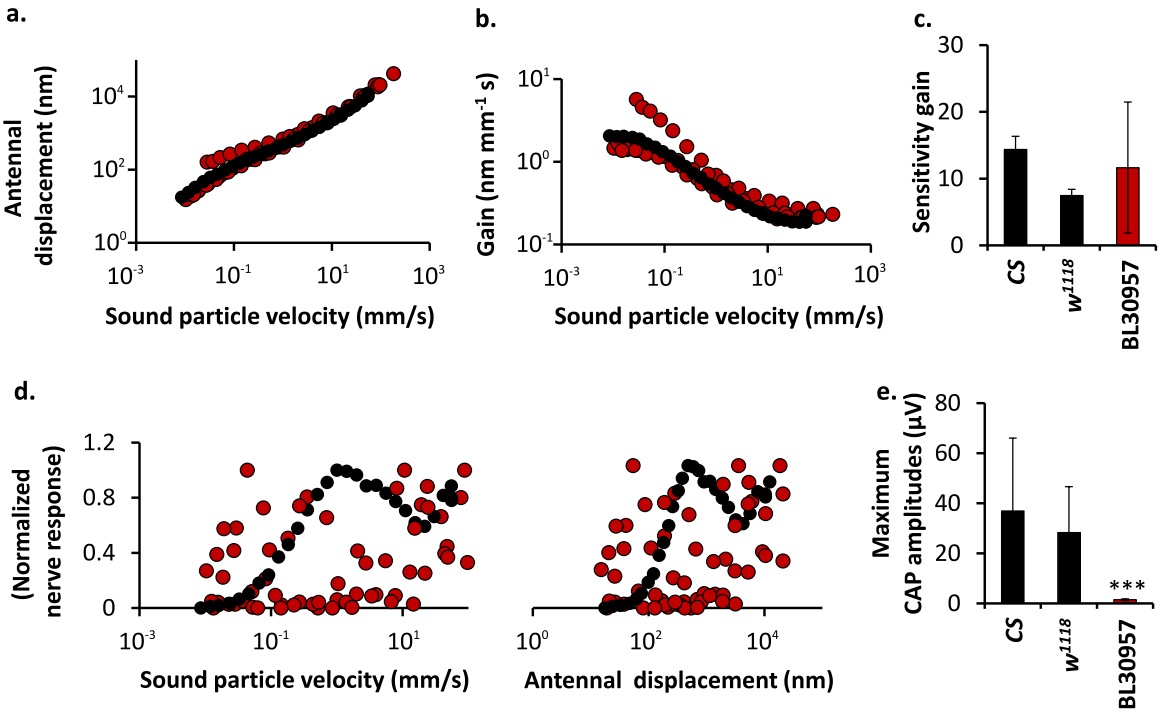

Fig. 3.15: Antennal mechanics and sound-evoked nerve response in BL30957. a and b. Nonlinear compression and power gain are seen when antennal displacements are plotted against sound particle velocities. c. Gain of BL30957 flies are found comparable with control flies. d and e. No sound-evoked CAP response can be detected in BL30957 flies. The black dots in a, b and d denote the wild-type responses. N≥4. ***p<0.01 (Student's t-test).

We checked the morphology of the JO neurons in the mutants by HRP staining (Fig. 3.16a). Expression of the TRP channels was checked by antibody staining against NOMPC and IAV (Fig. 3.16b). The gross neuronal morphology and TRP channels' expression along the length of the cilium look comparable to that of wild type flies. Thus, dm*dnah3* does not seem to control NOMPC localization unlike dm*dnai2*.

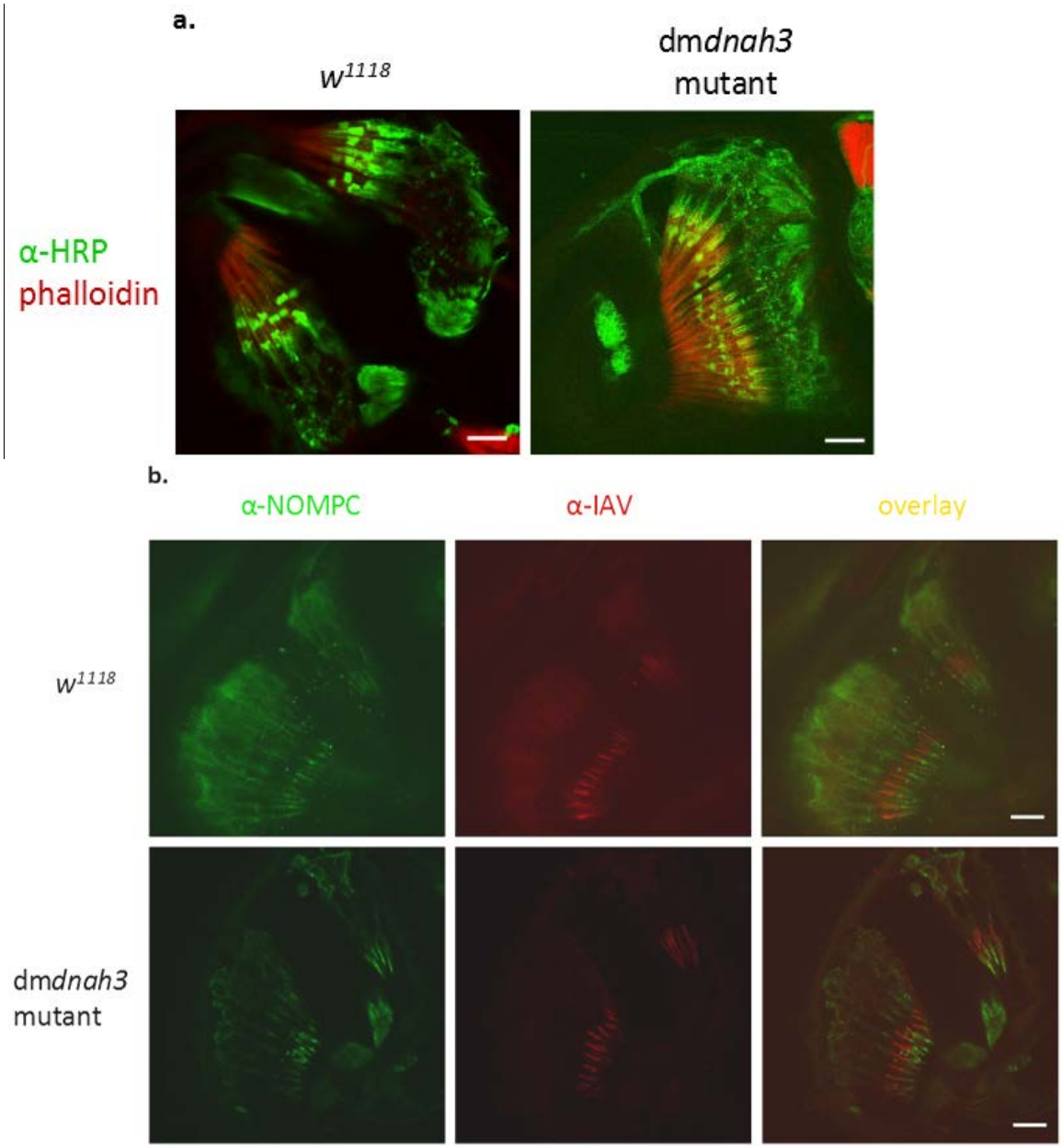

Fig. 3.16: Gross neuronal morphology and expression TRP channels in the JO neurons of dm*dnah3* mutants. a. The JO neurons of w^{1118} and dm*dnah3* mutant flies are stained with HRP (shown in green) and the scolopale cells with

phalloidin (shown in red). b. Antibody staining against NOMPC and IAV are shown in green and red respectively in w^{1118} and dm*dnah3* mutants. Scale bar: 10 µm.

Since amplification and expression of mechanotransducing and modulatory ion channels are intact in these flies it strongly suggests that the machinery responsible for mechanotransduction is still functional. Thus, absence of sound-evoked compound action potentials in these flies hints towards the role of dm*dnah3* in propagation of signals along the length of ciliated dendrites but not at the site of mechanotransduction. Since the TRPV channels are also expressed in the mutants it suggests a role of dm*dnah3* independent or downstream of the TRPV channels in sound-evoked action potential generation.

The mutant analyses suggest that dm*dnai2* might have a role in positive regulation of force generation and active amplification in the auditory neurons of *Drosophila melanogaster* while dm*dnah3* has roles in frequency tuning of the JO neurons and generation of sound-evoked antennal nerve response though not required in mechanotransduction in fly auditory neurons.

3.2 Expression of axonemal dyneins in the fly auditory system:

Though electron microscopic analyses suggest presence of dynein arms in the dendritic cilia of the JO neurons (Fig. 1.1f-h) no evidence has been shown to support their molecular identity. Previous work in the lab by Senthilan *et al* showed expression of *dhc93ab* and *CG9313* in the JO neurons indicating expression of axonemal dynein genes in the fly auditory system (Senthilan *et al*, 2012).

3.2.1 Promoter fusion construct expression of axonemal dynein genes in the fly auditory neurons:

Expression of dm*dnai2* and dm*dnah3* in the JO neurons was checked by generating promoter fusion constructs expressing GAL4 that was used to drive Green Fluoroscent Protein (GFP). Most of the JO neurons seem to be marked by promoter fusion constructs of both dm*dnai2* and dm*dnah3*. However, there are some neurons stained by neuronal marker FUTSCH (using 22c10 antibody) which are unmarked by the promoter fusion construct of dm*dnai2* (marked by white arrow in fig. 3.17a). This supports the fact that there is a remnant nerve response in the dm*dnai2* Minos insertion mutants and which might be due to firing of neurons which do not require the functioning of dm*dnai2* gene. Whereas since we never observed any JO neuron unmarked by dm*dnah3 Gal4* line and there is absolute abolishment of sound-evoked nerve response in the dm*dnah3* Minos insertion mutants it supports the idea that dm*dnah3* gene is required in all JO neurons.

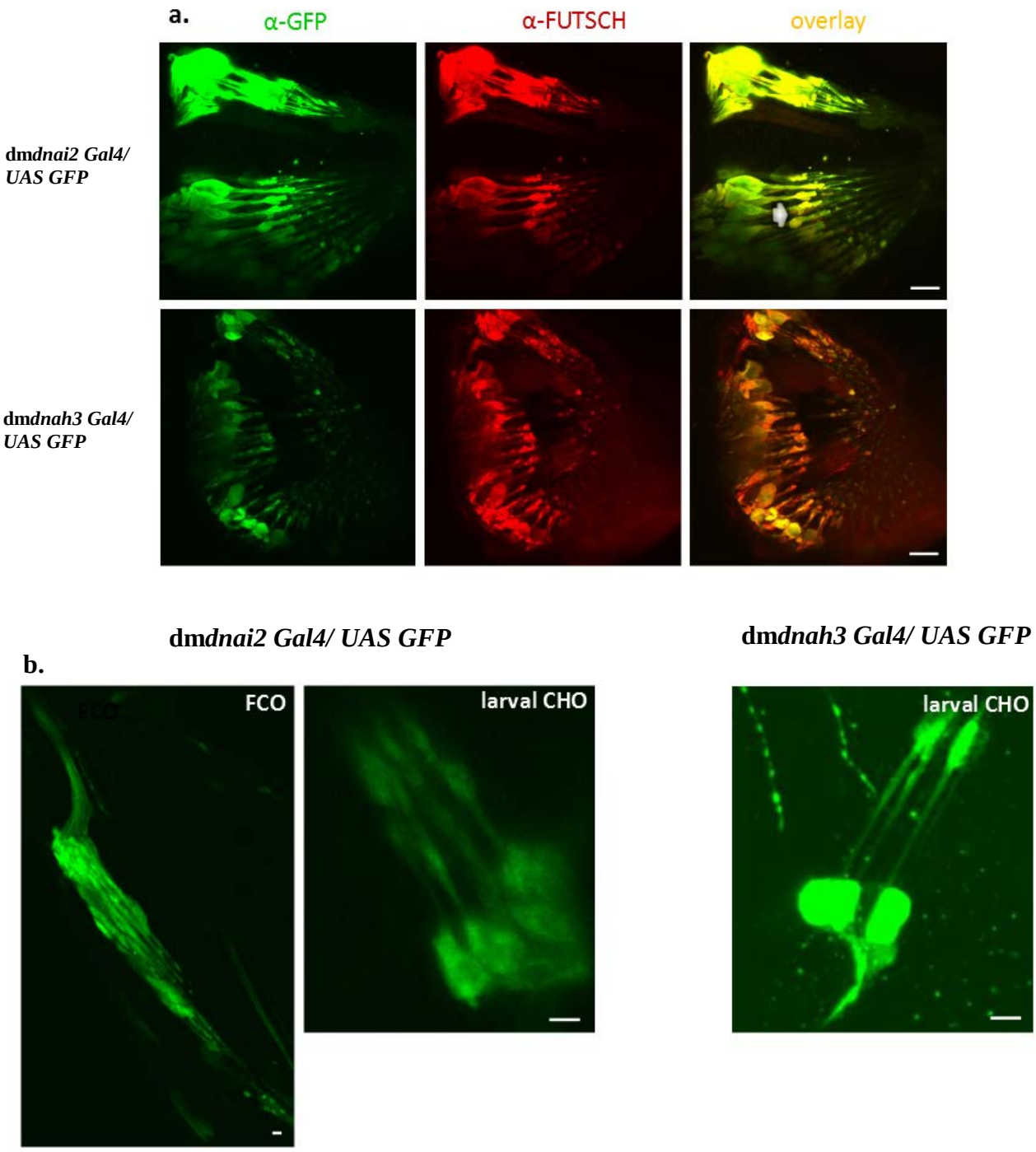

Fig. 3.17: Promoter fusion construct expression of *dmdnai2* and *dmdnah3*. a. *GFP* driven by *Gal4* lines of dm*dnai2* and dm*dnah3* shows expression in JO neurons. GFP is shown is green and neurons are marked by anti-FUTSCH staining (shown in red). The neurons marked by anti-FUTSCH but not by the dm*dnai2 Gal4* line are marked by a white arrow. Scale bar: 10 µm. b. Expression of dm*dnai2* and dm*dnah3 Gal4* line in the other chordotonal organs, namely the FCO and the larval CHO respectively. Scale bar: 5 µm.

The dm*dnai2 Gal4* line also shows expression in the FCO neurons and larval chordotonal organs but not in the bristles or campaniform sensilla. Likewise the dm*dnah3 Gal4* line also shows expression in the larval chordotonal organs. However, owing to our

constraints with slicing the leg femoral region and inability to perform immunohistochemistry in intact flies we could not perform antibody staining on the dm*dnah3* leg FCO. And unlike the dm*dnai2 Gal4* line, which is strong enough to be used for studying expression pattern without immunohistochemistry, dm*dnah3 Gal4* does not offer such possibilities. Hence, it is still to be checked if the dm*dnah3 Gal4* expresses in the leg FCO. Taken altogether the expression pattern of the two genes matches well with the expression pattern expected from an axonemal dynein, i.e unlike cytoplasmic motor proteins, it expresses only in the ch organ neurons but not in es organs.

Localization of axonemal dyneins (dmDNAI2) in the auditory neurons:

As dm*dnai2* seems to play a role in active amplification in the fly auditory system it was interesting to study localization of this protein. In order to do so a *UAS YFP*-tagged line of dm*dnai2* cDNA was generated. When the *YFP-tagged* dm*dnai2* is expressed under the *nan* promoter using *F- Gal4* line, in the dm*dnai2* Minos insertion mutant background it rescues the mutant phenotype and the flies thus, show active amplification and JO neurons regain their sensitivity towards sound stimuli (Fig. 3.18).

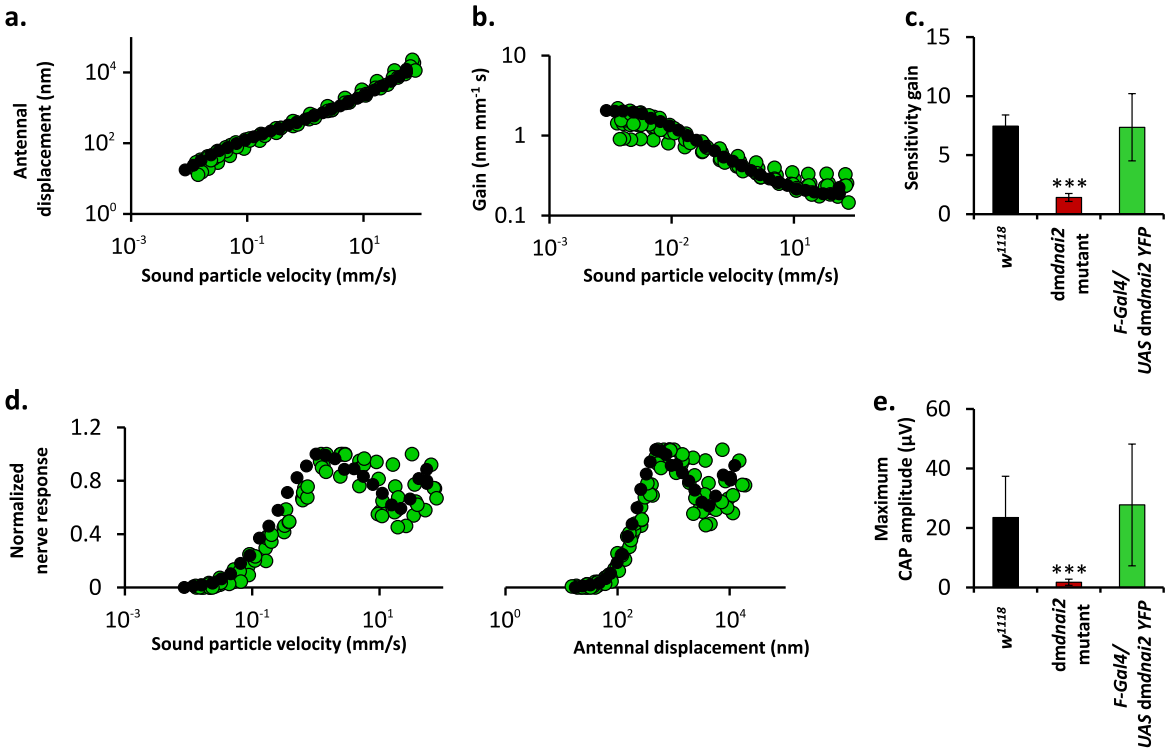

Fig. 3.18: Antennal mechanics and sound-evoked nerve response is regained in dm*dnai2* mutants when YFP-tagged dmDNAI2 is expressed in the JO neurons of the mutants. a and b. Nonlinear amplification is observed in the dm*dnai2* mutants when *YFP-tagged* dm*dnai2* is expressed by *F-Gal4*. c. Sensitivity gain of the mutants revert to normal by expression of YFP-tagged dmDNAI2. d and e. Sound-evoked nerve response in *dmdnai2* mutants become

comparable to control flies when YFP-tagged dmDNAI2 is expressed in the JO neurons. The black dots in a, b and d denote the wild-type responses. N≥5. ***p<0.01 (Student's t-test).

When the *UAS YFP-tagged* dm*dnai2* is expressed using the dm*dnai2 Gal4* line expression of YFP-tagged dmDNAI2 was observed in the proximal part of the dendrites of the JO neurons. (Fig. 3.19) It colocalizes with expression of TRPV channel, IAV as shown by its antibody staining (Fig. 3.19) and previous studies have shown that IAV exists as a heteromer with NAN (Gong *et al*, 2004).

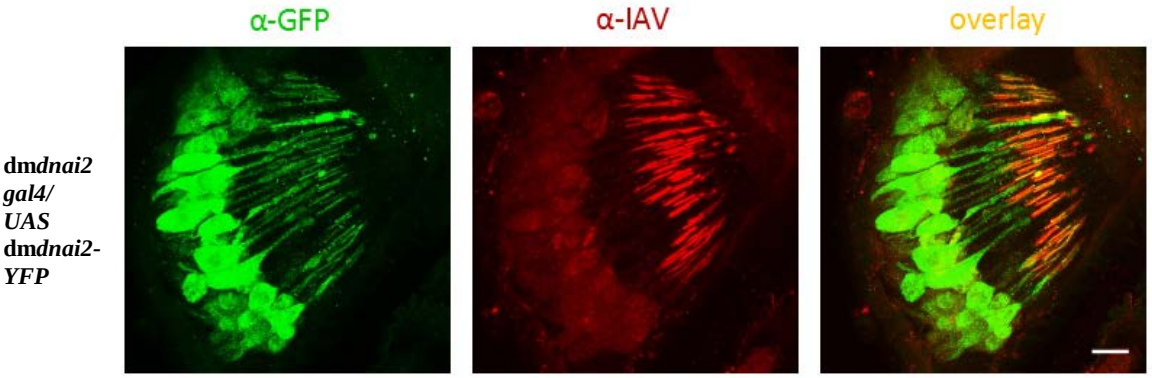

Fig. 3.19: Sub-cellular localization of dmDNAI2 in the JO neurons. *YFP-tagged UAS* dm*dnai2* construct was generated and was expressed using dm*dnai2 Gal4* line. YFP-tagged dmDNAI2 is stained using anti-GFP (shown in green) while IAV channels are stained using anti-IAV (shown in red). Scale bar: 10 µm.

It is interesting to note dmDNAI2 is not expressed in the distal tip of the neurons with NOMPC. However, our earlier results have shown that it still regulates the localization of NOMPC (Fig. 3.11). It is highly plausible that such control of NOMPC localization is mediated by ciliary movements and force generation than by direct interaction between NOMPC and axonemal dyneins.

3.3 Epistatic relation between axonemal dyneins and TRPV channels in the fly auditory system.

The co-localization of dmDNAI2 and IAV along the outer dendritic segment of the cilia (Fig. 3.19) suggests that axonemal dyneins might be required in a common pathway with the TRPV channels in the JO neurons. TRPV channels in the JO neurons are known to be heteromers of NAN and IAV (Gong *et al*, 2004) and are required for negative modulation of active amplification (Göpfert *et al*, 2006). Studies have shown that TRPV channels in JO neurons act upstream of TRPN1 (NOMPC) channels in the regulatory pathway that modulates mechanical amplification (Göpfert et al, 2006). However, in the transduction pathway, TRPVs act downstream of TRPN1 (Göpfert et al, 2006). TRPVs seem to regulate amplification via TRPN1, but how this regulation is accomplished is not understood.

To test for the relation between TRPVs and dyneins, double mutants were generated and epistatic analyses were performed: Epistasis allows one to predict the functional placement of genes in a pathway by using null mutants. It suggests that when two genes acting in the same pathway are mutated together the phenotype of such a double mutant will mimic the single mutation of the gene that acts more downstream in the pathway. If the two genes are involved in different pathways leading to the same phenotype, then the double mutant's phenotype is an additive effect of the two. Dm*dnai2*-iav^{1} and dm*dnah3*-nan^{dy5} double mutants were generated. The TRPV channel mutations that were used are nan^{dy5} and iav^{1}, which both are reportedly nulls. Whether nan or iav is used is not significant as null mutations in either of them abolishes the other.

Consistent with previous results nan^{dy5} and iav^{1} mutants displayed excess amplification (Fig. 3.20). However, both the double mutants of axonemal dyneins and TRPV channels showed amplification gains that resembled those observed in the single dynein mutant flies. The dm*dnai2* and iav^{1} double mutant showed lack of power in the system and complete loss of active amplification like the dm*dnai2* mutants themselves. Iav^{1} mutants show oscillations at about 118Hz and show peaks at the other harmonics of the resonant frequency. They show excess amplification and a ~70-fold power gain (Fig. 3.20). Both dm*dnai2* single mutants and *iav*-dm*dnai2* double mutants lack amplification. They show an antennal best frequency much shifted in the higher regime and power gain drops to 1.4 and 1.3 respectively (Fig. 3.20).

The dm*dnah3* and *nan*^{dy5} double mutant, by contrast, showed normal power spectra and amplification, like the dm*dnah3* mutants themselves (Fig. 3.20).

Nan^{dy5} mutants show antennal mechanics similar to the *iav*^{1} mutants. The antennae are tuned to lower best frequencies of about 107 Hz and they show a 52-fold power gain in the system. On the other hand, the dm*dnah3* single mutant and the *nan* ^{dy5}-dm*dnah3* double mutants show antennae tuned to best frequencies at around 302 Hz and 308 Hz respectively. Flies of both these genotypes also show an additional frequency to which the antennae show high tuning at about 800-1000 Hz. The gains in both the systems are quite comparable as well (the values being 19 and 25 respectively).

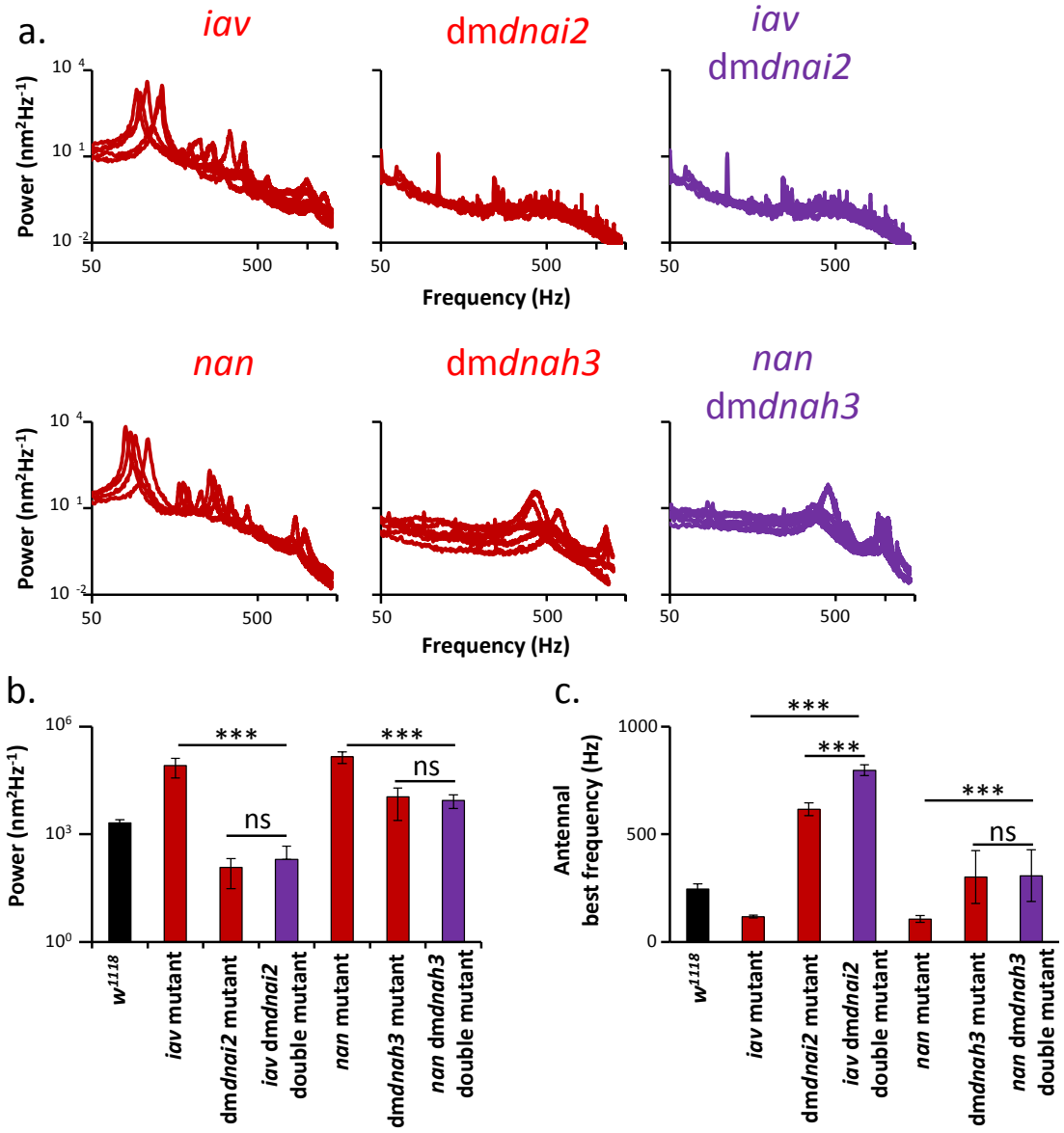

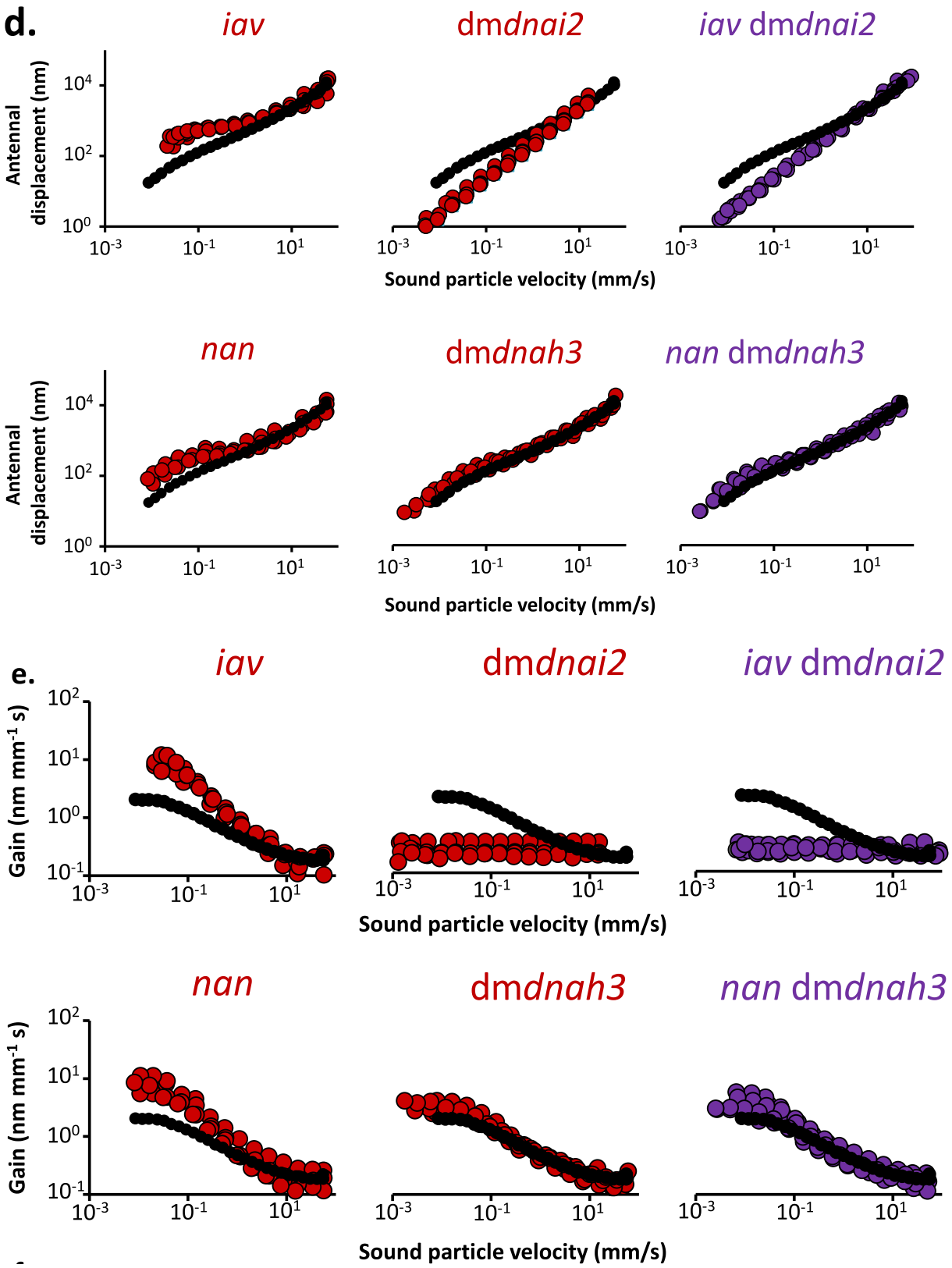
d.
iav
dmdnai2
iav dmdnai2
Antennal displacement (nm)
Sound particle velocity (mm/s)
nan
dmdnah3
nan dmdnah3
e.
Gain (nm mm-1 s)

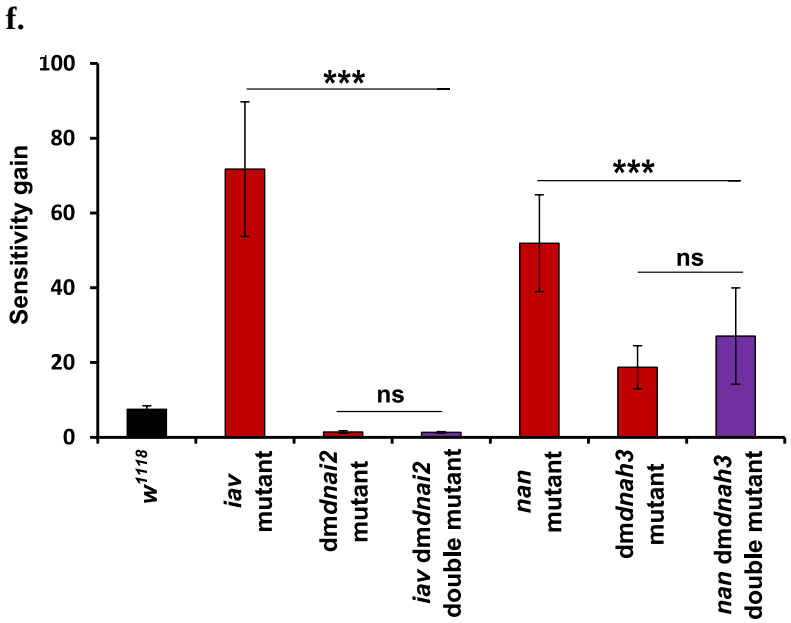

Fig. 3.20: Biomechanical analyses of double mutants of axonemal dyneins and TRPV channels. a. Power spectra of antennae of each genotype is plotted against frequency. b and c. Total power and best frequency is plotted for each genotype respectively. d and e. Antennal displacements and gain for each genotype are plotted against sound particle velocity respectively. f. Sensitivity gain for each genotype is plotted. ***denotes p<0.01 (Student's t-test).

The similarity of the phenotypes of both the TRP-dynein double mutant is similar to the respective dynein single mutants. This places the two dyneins downstream of TRPV channels in the regulatory pathway that modulates amplification, demonstrating that TRPVs require axonemal dyneins to regulate the amplification gain. While dm*dnai2* seems to be a part of the force generator leading to active amplification, which is under negative modulation of TRPV. On the other hand dm*dnah3*, though is not required for normal amplification seems to be required in force regulation in TRPV mutants. Thus, dm*dnah3* seems to play a modulatory role under the control of TRPV in force generation by the fly auditory neurons. This leads us to make a generalization that TRPVs control axonemal dyneins (Fig. 3.21).

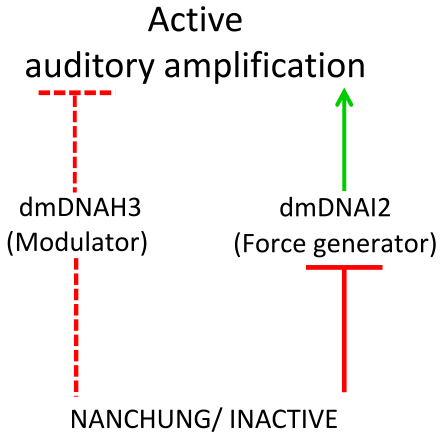

Fig. 3.21: Model explaining the interaction between TRPV channels and axonemal dyneins in regulation of active auditory amplification. Epistatic analyses results suggest that TRPV channels negatively modulate dmDNAI2 (force generator) and thus maintain a negative feedback on active amplification in the JO neurons. DmDNAH3 (modulator) seems to be under direct positive control of TRPV channels.

4. Discussion.

Like vertebrate hair cells, *Drosophila* JO neurons are motile and serve dual, transducing and actuating roles. Mechanistically, the motility of JO neurons resembles the active hair bundle motility of vertebrate hair cells: like this hair bundle motility, that of JO neurons can be quantitatively explained by an active version of the gating spring model (Nadrowski *et al*, 2004, Nadrowski *et al*, 2008). According to this model, the motile properties arise from the interplay between the gating of the transduction channels and associated movements of adaptation motors.

Profiting from the amenability of *Drosophila* to genetic dissection, this thesis aimed to identify motor proteins in the neurons of JO that are implicated in their motility. The mere presence of dynein-like arms in the mechanosensory cilia of these neurons suggests that amplification might in involve axonemal dynein motors. Previous studies had also shown that amplification is abolished in mutant flies where the dynein-like arms are lost (Kavlie et al, 2010). The presence of axonemal dynein arms in the cilia would be interesting: judging from their 9+0 axonemes, the cilia of JO neurons are primary cilia that usually lack dynein arms and are immotile. The only motile primary cilia that have been described so far are the nodal cilia, which also bear dynein arms (Hirokawa *et al*, 2009).

The aim of this thesis was to determine whether axonemal dynein arm components are expressed in JO neurons and to evaluate their role for their motility. By homology screening, all the known axonemal dyneins of the fly were identified and auditory phenotypes of available mutants that were examined. Then, two axonemal dyneins were selected and their requirements for motility were studied in more detail. Mutant analyses revealed that most of the axonemal dynein proteins that we studied serve different roles in neurons of JO.

As shown by expression of the promoter fusion axonemal dyneins are expressed only in ch organ neurons, but not in es neurons whose cila have not yet been reported to display dynein-like arms. In the ch neurons of JO, the YFP-tagged dmDNAI2 localizes to the proximal ciliary region, where it co-localizes with TRPV channels. Judging from EM

studies (personal communication with Dr. Daniel Eberl, University of Iowa), dynein-like arms are confined to this ciliary region, supporting the hypothesis that these arms are formed by dyneins.

Promoter fusion constructs suggest that dm*dnai2* is expressed in most but not all the 500 JO neurons. Consistently, the respective mutants generated residual electrical nerve potentials when stimulated with loud sounds. Judging from their intensity-characteristics, these residual sound responses might originate from gravity/wind-sensitive JO neurons, which only respond to high intensity sounds (Effertz *et al*, 2011). Whether dm*dnai2* expression is absent from CE neurons remains to be tested. If so, this would mean that some axonemal dyneins are confined to certain JO neurons, maybe those auditory neurons that are specifically required for active amplification in the fly (Effertz *et al*, 2011).

Promoter fusion construct of dm*dnah3*, by contrast, seems to mark all the JO neurons and the mutants show a complete loss of the sound-evoked nerve response. Since the mutants show intact amplification, this gene is not required for the amplification of the low intensity sound stimuli, but seems to be required for downstream electrical signal propagation. In addition, dm*dnah3* seems to have a role in frequency tuning : in the mutants, the antenna's frequency response displays two peaks instead of only one. More work will be needed to assess the tuning mechanisms of JO neurons: Previous studies revealed that different neuronal subpopulations differ in their frequency characteristics (Kamikouchi *et al*, 2009), yet how these different frequency characteristics are brought about and how dyneins contribute to this, still remains unknown.

Dm*dnai2* mutants show a mislocalization of NOMPC channel into the proximal region of the JO neurons. This phenotype is seen in *fd3f* mutants as well (Newton *et al*, 2012). *Fd3f* is a transcription factor that is required for the differentiation of ch neurons, regulating many genes that encode proteins that localize to the proximal region of the cilium. The list of genes controlled by *fd3f* includes axonemal dyneins (including dm*dnai2*) and also TRPV channels. Since *fd3f* mutants lack axonemal dyneins and show mislocalization of NOMPC it seems that *fd3f* might regulate or maintain NOMPC localization via axonemal dyneins. Es neurons, which lack the dyneins and also dynein-like arms also express the

NOMPC channel. Should the dyneins participate in NOMPC localization, this role would be confined to the chordotonal neurons of the fly.

According to the results of this thesis, also the dynein heavy chain *dhc62b* modulates the amplification gain. Mutations in *dhc62b* cause hyperamplification that is even more pronounced that that seen in flies carrying mutations in dm*dnah3*. Hyperamplication also characterizes TRPV channel mutants, in which the negative regulation of amplification is disturbed (Göpfert et al., 2006). Judging from double mutants, TRPV channels negatively control amplification via NOMPC (Göpfert et al., 2006). *Dhc62b* might act together with TRPV channels in this regulation, or, alternatively, act in a second regulatory pathway that does not involve TRPVs, which needs to be checked.

The former, one pathway scenario is, however, supported here for dm*dnai2* and dm*dnah3* by epistatic analyses using double mutants. To test for epistasis, double mutants were generated for dm*dnai2* and dm*dnah3* with *iav* and *nan* respectively: in chordotonal neurons, the Nan and Iav, the fly's two TRPVs, seem to form a heterodimeric Nan-Iav channel, and mutations in each of the corresponding genes abolish both TRPV proteins (Gong *et al*, 2004). For both dyneins, similar epistatic relations were observed with TRPVs, indicating that they operate in common pathway that regulates the amplificatory gain. Within this pathway, the two dyneins are placed downstream of TRPVs, thus, indicating that TRPVs negatively regulate the amplificatory gain through dyneins. Possibly, signaling through TRPV channels inactivates dynein motor components and mediates its negative modulation on active amplification. How exactly TRPVs might signal to dyneins, however, is unclear: when expressed heterologously, Nan and Iav reportedly form calcium-permeable channels (Kim *et al*, 2003). In Senthilan et al, 2012, however, it was shown that calmodulin mutants show excess amplification. Thus, it leads to the prediction that calcium signaling might negatively regulate the force generators in the JO neurons. One might also speculate that the TRPVs and the axonemal dyneins directly interact, which would seem plausible- given that the dynein-like arms are close and maybe connected to the ciliary membrane, and that both dyneins and TRPVs localize to the same region of the cilium.

Experiments by Goswami et al, 2004 suggest that conserved amino acid motifs on the C-termini of TRPV channels interact with microtubules via ß-tubulin in a Ca^{+2} dependent

manner. It remains to be checked if such conserved amino acid motifs are present in the fly's TRPVs. If so, it will be interesting to see whether they interact with tubulins as well. Such interaction would be interesting: in that case, calcium entering through TRPVs could signal to the dyneins via tubulins, providing a potential signaling mechanism for the activation or inactivation of dyneins.

Given that axonemal dyneins are motor proteins that confer ciliary motility, it seems possible that serve as adaptation motors in the auditory neurons of the fly: as was outlined above, amplification by the fly's auditory neurons seems linked to auditory stimulus transduction, whereby adaptation motors seem to provide the energy. In axonemal dynein complexes, the components that convert ATP into mechanical energy are heavy chains. The heavy chain that this thesis focuses on, dm*dnah3*, is not required for amplification and, accordingly, unlikely to act as adaptation motors in the fly. A better candidate seems to be the axonemal dynein heavy chain dm*dnai2*, which is required for active amplification in the fly.

If dyneins should act as the adaptation motors, this would suggest that the transduction channels also reside in the proximal region of the cilium. A potential candidate are the TRPV channels proper, whose loss seem to largely abolish transduction currents in the neurons of JO (Lehnert et al. 2013). Another candidate for the transduction channel is NOMPC, which seems to act as a force-gated channel at the ciliary tip (Effertz et al., 2012, Jan paper 2013). Judging from force-gating studies, NOMPC is an adapting ion channel (Albert et al., 2007, Effertz et al., 2012) so if dyneins are the respective motors their movements would need to adapt the NOMPC channels in the ciliary tips. Such special segregation of channels and motors would be reminiscent of the situation in hair cells, were both components seem to sit in adjacent sterocilia (Beurg *et al*, 2009). In the fly, microtubules could communicate between dyneins and NOMPC, given that NOMPC binds to microtubules with its N-terminus (Cheng *et al*, 2010).

Axonemal dyneins were shown to be expressed in Johnston's organ neurons, where they localize to the proximal region of the cilia. This ciliary region presents dynein arm-like structures, which, according to the data presented here, are likely formed by dyneins. Mutant analysis has shown that dyneins are required for the motility of JO neurons, and the active amplification that these cells exert. Axonemal dyneins were also shown to

control this motility, regulating the amplificatory gain together with TRPVs. In addition, dyneins seem to function in electrical downstream electrical signal propagation, where they also seem to work in concert with TRPVs. Taken together, these findings document multiple roles of axonemal dyneins in the fly hearing, and raise the possibility that the predicted adaptation motors that are thought to promote amplification in the fly's auditory system are also axonemal dyneins. If so, flies and vertebrates would seem to use different types of motor proteins for auditory transduction channel adaptation, even though their transduction apparatuses operate in a very similar way. Functional, but not molecular equivalence, also seems to exist with respect to the auditory transduction channels, which, in the fly seem to be TRP channel family members but in vertebrates might be TMCs (Kawashima *et al*, 2011, Pan *et al*, 2013).

Controversy has arisen on whether NOMPC or TRPVs are the fly's auditory transduction channels: NOMPC is a bona fide mechanotransduction channel (Yan *et al*, 2013) that, in the fly's auditory JO neurons, is required for amplification (Göpfert et al. 2006) and transducer gating (Effertz et al, 2012), yet it might that most of the transduction currents is nonetheless generated by ions entering through the TRPVs (Lehnert et al. 2013). The idea of two transduction channels might operate in series might seem surprising, yet it seems possible given that both these channels might be mechanically coupled through the cilium. Such coupling could provide a mechanism by which dyneins might drive the adaptation of the NOMPC channels in the distal region of the cilium.

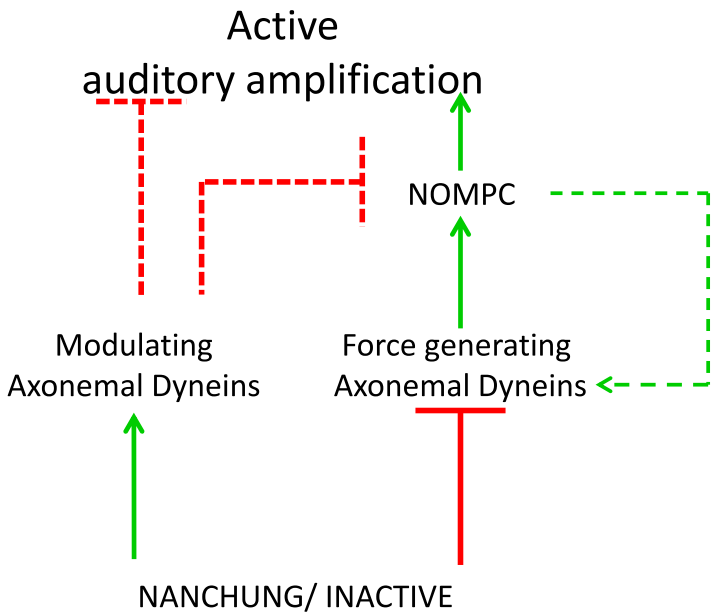

Fig. 3.22: Model explaining the interaction between TRP channels and axonemal dyneins in force generation by fly auditory neurons. At least functionally two different types of axonemal dyneins seem to be expressed in the JO neurons in *Drosophila melanogaster*, force generators and modulators. Our results support that TRPVs negatively regulate the force generators while positively regulating the modulatory axonemal dyneins. It can be predicted that there might be a positive mechanical feedback from NOMPC residing at the tip of the neurons with the force generating axonemal dyneins in the proximal region of the cilia. However, it still remains to be seen if the modulatory axonemal dyneins act via NOMPC or independently in the pathway of force generation.

5. References.

1. **Ainsley, J. A., J. M. Pettus, D. Bosenko, C. E. Gerstein, N. Zinkevich, M. G. Anderson, C. M. Adams, M. J. Welsh and W. A. Johnson (2003)**. "Enhanced Locomotion Caused by Loss of the Drosophila DEG/ENaC Protein Pickpocket1." Current Biology 13(17): 1557-1563.
2. **Albert, J. T., B. Nadrowski and M. C. Göpfert (2007).** "Mechanical Signatures of Transducer Gating in the Drosophila Ear." Current Biology 17(11): 1000-1006.
3. **Bechstedt, S., Albert, J. T., Kreil, D. P., Müller-Reichert, T, Göpfert, M. C., Howard, J (2010).** "A doublecortin containing microtubule-associated protein is implicated in mechanotransduction in Drosophila sensory cilia." Nat Commun.
4. **Beurg, M., R. Fettiplace, J.-H. Nam and A. J. Ricci (2009).** "Localization of inner hair cell mechanotransducer channels using high-speed calcium imaging." Nat Neurosci 12(5): 553-558.
5. **Cachero S, S. T., Zur Lage PI, Ma L, Newton FG, Holohan EE, Armstrong JD, Jarman AP.** (2011). "The gene regulatory cascade linking proneural specification with differentiation in Drosophila sensory neurons." PLoS Biol.
6. **Campuzano, S. and J. Modolell (1992).** "Patterning of the Drosophila nervous system: the achaete-scute gene complex." Trends in Genetics 8(6): 202-208.
7. **Cheng, L. E., W. Song, L. L. Looger, L. Y. Jan and Y. N. Jan (2010).** "The Role of the TRP Channel NompC in Drosophila Larval and Adult Locomotion." Neuron 67(3): 373-380.
8. **Choe Y, M. M., Hudspeth AJ. (1998).** "A model for amplification of hair-bundle motion by cyclical binding of Ca2+ to mechanoelectrical transduction channels." Proc. Natl. Acad. Sci. USA.
9. **Chung, Y. D., J. Zhu, Y.-G. Han and M. J. Kernan (2001).** "nompA Encodes a PNS-Specific, ZP Domain Protein Required to Connect Mechanosensory Dendrites to Sensory Structures." Neuron 29(2): 415-428.
10. **Cyr, J. L., R. A. Dumont and P. G. Gillespie (2002).** "Myosin-1c Interacts with Hair-Cell Receptors through Its Calmodulin-Binding IQ Domains." The Journal of Neuroscience 22(7): 2487-2495.

11. **Effertz, T., R. Wiek and Martin C. Göpfert (2011).** "NompC TRP Channel Is Essential for Drosophila Sound Receptor Function." Current Biology 21(7): 592-597.
12. **Effertz, T., B. Nadrowski, D. Piepenbrock, J. T. Albert and M. C. Gopfert (2012).** "Direct gating and mechanical integrity of Drosophila auditory transducers require TRPN1." Nat Neurosci 15(9): 1198-1200.
13. **Fichelson, P. and M. Gho (2003).** "The glial cell undergoes apoptosis in the microchaete lineage of Drosophila." Development 130(1): 123-133.
14. **Goldschmidt, R. B. and O. Steward (1989).** "Comparison of the neurotoxic effects of colchicine, the vinca alkaloids, and other microtubule poisons." Brain Research 486(1): 133-140.
15. **Gong J, W. Q., Wang Z. (2013).** "NOMPC is likely a key component of Drosophila mechanotransduction channels." Eur J Neurosci. .
16. **Gong, Z., W. Son, Y. Doo Chung, J. Kim, D. W. Shin, C. A. McClung, Y. Lee, H. W. Lee, D.-J. Chang, B.-K. Kaang, H. Cho, U. Oh, J. Hirsh, M. J. Kernan and C. Kim (2004).** "Two Interdependent TRPV Channel Subunits, Inactive and Nanchung, Mediate Hearing in Drosophila." The Journal of Neuroscience 24(41): 9059-9066.
17. **Göpfert , M. C. and Robert D. (2002).** "The mechanical basis of Drosophila audition." The Journal of Experimental Biology.
18. **Göpfert, M. C. and D. Robert (2003).** "Motion generation by Drosophila mechanosensory neurons." Proceedings of the National Academy of Sciences 100(9): 5514-5519.
19. **Gopfert, M. C., J. T. Albert, B. Nadrowski and A. Kamikouchi (2006).** "Specification of auditory sensitivity by Drosophila TRP channels." Nat Neurosci 9(8): 999-1000.
20. **Goswami C, D. M., Jahnel R, Bogen O, Gillen C, Hucho F. (2004).** "Identification and characterization of a Ca2+ -sensitive interaction of the vanilloid receptor TRPV1 with tubulin." J Neurochem. .
21. **Hartenstein, V. (1988).** "Development of Drosophila larval sensory organs: spatiotemporal pattern of sensory neurons, peripheral axonal pathways and sensilla differentiation." Development(107): 389–405.
22. **Hirokawa, N., Y. Tanaka and Y. Okada (2009).** "Left–Right Determination: Involvement of Molecular Motor KIF3, Cilia, and Nodal Flow." Cold Spring Harbor Perspectives in Biology 1(1).

23. **Holt, J. R., S. K. H. Gillespie, D. W. Provance Jr, K. Shah, K. M. Shokat, D. P. Corey, J. A. Mercer and P. G. Gillespie (2002).** "A Chemical-Genetic Strategy Implicates Myosin-1c in Adaptation by Hair Cells." Cell 108(3): 371-381.
24. **Höök, P. and R. B. Vallee (2006).** "The dynein family at a glance." Journal of Cell Science 119(21): 4369-4371.
25. **Hudspeth, A. J., Y. Choe, A. D. Mehta and P. Martin (2000).** "Putting ion channels to work: Mechanoelectrical transduction, adaptation, and amplification by hair cells." Proceedings of the National Academy of Sciences 97(22): 11765-11772.
26. **Jarman, A. P., Y. Grau, L. Y. Jan and Y. N. Jan (1993).** "atonal is a proneural gene that directs chordotonal organ formation in the Drosophila peripheral nervous system." Cell 73(7): 1307-1321.
27. **Jarman, A. P., Y. Sun, L. Y. Jan and Y. N. Jan (1995).** "Role of the proneural gene, atonal, in formation of Drosophila chordotonal organs and photoreceptors." Development 121(7): 2019-2030.
28. **Kamikouchi, A., H. K. Inagaki, T. Effertz, O. Hendrich, A. Fiala, M. C. Gopfert and K. Ito (2009).** "The neural basis of Drosophila gravity-sensing and hearing." Nature 458(7235): 165-171.
29. **Kamikouchi, A., R. Wiek, T. Effertz, M. C. Gopfert and A. Fiala (2010).** "Transcuticular optical imaging of stimulus-evoked neural activities in the Drosophila peripheral nervous system." Nat. Protocols 5(7): 1229-1235.
30. **Kavlie, R. G., M. J. Kernan and D. F. Eberl (2010).** "Hearing in Drosophila Requires TilB, a Conserved Protein Associated With Ciliary Motility." Genetics 185(1): 177-188.
31. **Kawashima, Y., Geleoc GS, K. Kurima, V. Labay, A. Lelli, Y. Asai, T. Makishima, D. K. Wu, C. C. Della Santina, J. R. Holt and A. J. Griffith (2011).** "Mechanotransduction in mouse inner ear hair cells requires transmembrane channel–like genes." The Journal of Clinical Investigation 121(12): 4796-4809.
32. **Kernan, M. (2007).** "Mechanotransduction and auditory transduction in Drosophila." Pflügers Archiv - European Journal of Physiology 454(5): 703-720.
33. **Kim, J., Y. D. Chung, D.-y. Park, S. Choi, D. W. Shin, H. Soh, H. W. Lee, W. Son, J. Yim, C.-S. Park, M. J. Kernan and C. Kim (2003).** "A TRPV family ion channel required for hearing in Drosophila." Nature 424(6944): 81-84.

34. **King, S. M. (2010).** "Sensing the mechanical state of the axoneme and integration of Ca2+ signaling by outer arm dynein." Cytoskeleton 67(4): 207-213.
35. **King, S. M. (2013).** Chapter Eight - Biochemical and Physiological Analysis of Axonemal Dyneins. Methods in Enzymology. F. M. Wallace, Academic Press. Volume 524: 123-145.
36. **Lai, E. C. and V. Orgogozo (2004).** "A hidden program in Drosophila peripheral neurogenesis revealed: fundamental principles underlying sensory organ diversity." Developmental Biology 269(1): 1-17.
37. **Lehnert, Brendan P., Allison E. Baker, Q. Gaudry, A.-S. Chiang and Rachel I. Wilson (2013).** "Distinct Roles of TRP Channels in Auditory Transduction and Amplification in Drosophila." Neuron 77(1): 115-128.
38. **Liang X, M. J., Saleh HS, Howard J. (2011).** "NOMPC, a member of the TRP channel family, localizes to the tubular body and distal cilium of Drosophila campaniform and chordotonal receptor cells." Cytoskeleton (Hoboken).
39. **Mallik R and Gross S. P. (2004).** "Molecular motors: Strategies to get along." Current Biology (14): R971-R982
40. **MH, D. (1999).** "Haltere-mediated equilibrium reflexes of the fruit fly, Drosophila melanogaster." Philos Trans R Soc LondB Biol Sci (354:): 903–916.
41. **Mizuno, N., M. Taschner, B. D. Engel and E. Lorentzen (2012).** "Structural Studies of Ciliary Components." Journal of Molecular Biology 422(2): 163-180.
42. **Nadrowski, B., J. T. Albert and M. C. Göpfert (2008).** "Transducer-Based Force Generation Explains Active Process in Drosophila Hearing." Current Biology 18(18): 1365-1372.
43. **Nadrowski, B., P. Martin and F. Jülicher (2004).** "Active hair-bundle motility harnesses noise to operate near an optimum of mechanosensitivity." Proceedings of the National Academy of Sciences of the United States of America 101(33): 12195-12200.
44. **Newton, Fay G., Petra I. zur Lage, S. Karak, Daniel J. Moore, Martin C. Göpfert and Andrew P. Jarman (2012).** "Forkhead Transcription Factor Fd3F Cooperates with Rfx to Regulate a Gene Expression Program for Mechanosensory Cilia Specialization." Developmental Cell 22(6): 1221-1233.
45. **Nin, F., T. Reichenbach, J. A. N. Fisher and A. J. Hudspeth (2012).** "Contribution of active hair-bundle motility to nonlinear amplification in the mammalian cochlea." Proceedings of the National Academy of Sciences 109(51): 21076-21080.

46. **Orgogozo, V., F. Schweisguth and Y. Bellaïche (2002).** "Binary cell death decision regulated by unequal partitioning of Numb at mitosis." Development 129(20): 4677-4684.
47. **Pan, B., Gwenaelle S. Géléoc, Y. Asai, Geoffrey C. Horwitz, K. Kurima, K. Ishikawa, Y. Kawashima, Andrew J. Griffith and Jeffrey R. Holt (2013).** "TMC1 and TMC2 Are Components of the Mechanotransduction Channel in Hair Cells of the Mammalian Inner Ear." Neuron 79(3): 504-515.
48. **Pedersen, L. B. and S. T. Christensen (2012).** "Regulating intraflagellar transport." Nat Cell Biol 14(9): 904-906.
49. **Peng, A. W., F. T. Salles, B. Pan and A. J. Ricci (2011).** "Integrating the biophysical and molecular mechanisms of auditory hair cell mechanotransduction." Nat Commun 2: 523.
50. **Probst, R. (1990).** "Otoacoustic emissions: an overview." In: Pfaltz, CR., editor. New Aspects of Cochlear Mechanics and Inner Ear Pathophysiology.
51. **Roberts, Anthony J., B. Malkova, Matt L. Walker, H. Sakakibara, N. Numata, T. Kon, R. Ohkura, Thomas A. Edwards, Peter J. Knight, K. Sutoh, K. Oiwa and Stan A. Burgess (2012).** "ATP-Driven Remodeling of the Linker Domain in the Dynein Motor." Structure 20(10): 1670-1680.
52. **Ruggero MA, R. N. (1991).** "Application of a commercially-manufactured Dopplershift laser velocimeter to the measurement of basilar-membrane vibration." Hear Res.
53. **Ruggero MA, R. N., Recio A, Narayan SS, Robles L. (1997).** "Basilar-membrane responses to tones at the base of the chinchilla cochlea." J. Acoust. Soc.
54. **Senthilan, Pingkalai R., D. Piepenbrock, G. Ovezmyradov, B. Nadrowski, S. Bechstedt, S. Pauls, M. Winkler, W. Möbius, J. Howard and Martin C. Göpfert (2012).** "Drosophila Auditory Organ Genes and Genetic Hearing Defects." Cell 150(5): 1042-1054.
55. **Slepecky, N. (1996).** "Structure of the Mammalian Cochlea." (New York: Springer-Verlag.
56. **Tan, X., J. L. Pecka, J. Tang, S. Lovas, K. W. Beisel and D. Z. Z. He (2012).** "A motif of eleven amino acids is a structural adaptation that facilitates motor capability of eutherian prestin." Journal of Cell Science 125(4): 1039-1047.
57. **Warren, B., A. N. Lukashkin and I. J. Russell (2010).** "The dynein–tubulin motor powers active oscillations and amplification in the hearing organ of the mosquito." Proceedings of the Royal Society B: Biological Sciences 277(1688): 1761-1769.

58. **Yack, J. E. (2004).** "The structure and function of auditory chordotonal organs in insects." Microscopy Research and Technique 63(6): 315-337.
59. **Yan, Z., W. Zhang, Y. He, D. Gorczyca, Y. Xiang, L. E. Cheng, S. Meltzer, L. Y. Jan and Y. N. Jan (2013).** "Drosophila NOMPC is a mechanotransduction channel subunit for gentle-touch sensation." Nature 493(7431): 221-225.
60. **Zhong, L., R. Y. Hwang and W. D. Tracey (2010).** "Pickpocket Is a DEG/ENaC Protein Required for Mechanical Nociception in Drosophila Larvae" Current Biology 20(5): 429-434.

Acknowledgements:

I would like to take this opportunity to thank a number of people whose efforts have helped me immensely in the last four years of my doctoral thesis.

Huge thanks to Prof. Martin Göpfert for the opportunity to work on a topic of my interest as my PhD project in his lab and more importantly for the enthusiasm and academic freedom that he lets one maintain. A PhD tenure without such a privilege, I am sure would not have been half as enjoyable. At the same time I thank my thesis committee members, Prof. Andre Fiala and Prof. Tobias Moser and my collaborator Dr. Daniel Eberl, University of Iowa for their insights into my work.

The Göpfert lab members, both past and present, deserve heartfelt thanks for all the help I have received in various forms from them. I joined the lab without previous experience in most of the techniques pursued here. Though that gave me a chance to learn as much as I could I am sure many in the lab were patient enough to let me grow. My electrophysiology set up would not have been functional and ready had it not been for Thomas and Simon. Learning and getting used to a new field would not have been half as exciting had it not been more those engaging discussions with Bjorn, Georg, David, Simon, Philipp, Christian and Robert. Huge thanks to Seol hee, Marta and Damiano, for being the fellow molecular biologists and sharing the moments of frustrations when things don't work the way one wants them to. To Pingkalai, for the support and the guidance during the short overlap I had with her in the lab. To Maike, for without her electron microscopic studies of fly auditory system in our lab would not have taken a flight. To Steffi, Margret and Sylvia for their enormous technical assistance and emotional support. And a huge bunch of thanks for Gudrun, for her support and co-ordination and for making sure that I was not thrown out of the University or the country owing to my lack of administrative knowledge or laziness (or both most of the times). And certainly loads of thanks to the other members in the group for keeping the workplace atmosphere healthy and pleasant.

I was enormously lucky to always have gotten neighbourhood labs to take care of last minute panic situations, both while at MPI (EM) and at SSF. Heartfelt thanks to AG

Simons, AG Stegmueller, AG Fiala and AG Schlueter for having rescued many of my experiments! Many thanks to my Prof. Maurice Kernan, SUNY, Prof. Changsoo Kim, Chonnam National University , Dr. Yun Doo Chung, University of Seoul, Dr. April Marrone, MPI-BPC and Johanes Bishchof from Baseler lab, University of Zurich for their generous support with providing handy experimental reagents and to Dr. Carolin Wichmann for her incessant help to us with the electron microscopy.

I thank GGNB for having made sure that our PhD tenures run smooth. Thanks to the SMN program for all the retreats and all the scientific discussions that came with it, of course! On a more serious note, you made it sure that doing science is fun and desirable ☺. Loads of thanks to Neurosenses for funding me over the last three years. Without a support as generous as this moving into a new country and a new work culture would have been way more difficult to deal with.

And certainly loads of thanks and regards to my family and friends whose presence and unconditional support simplified many situations and the smile they brought along with.

***Curriculum vitae*:**

Personal information:
Name: Somdatta Karak
Date of birth: 25th September, 1985
Place of birth: Chandpatra, West Bengal, India
Nationality: Indian

Education:

2009- present	PhD student in Georg August Universität, Göttingen, Germany. Thesis titled: Axonemal dyneins and force generation in auditory neurons of *Drosophila melanogaster*. Committee members: Prof. Dr. Martin Göpfert (supervisor), Prof. Dr. Andre Fiala, Prof. Dr. Tobias Moser.
2006-2009	Masters in Biology (by Research) at Tata Institute of Fundamental Research, Mumbai, India. Supervisor: Prof. Dr. Veronica Rodrigues.
2003-2006	Bachelors in Biotechnology at V.G. Vaze College, University of Mumbai, India.

Publications:

Central synaptic mechanisms underlie short term olfactory habituation in *Drosophila* larvae. Larkin
A, **Karak S**, Priya R, Das A, Ayyub C, Ito K, Rodrigues V, Ramaswami M., Learn. & Mem. 2010.

Forkhead transcription factor Fd3F cooperates with Rfx to regulate a gene expression program for mechanosensory cilia specialization. Newton FG, zur Lage PI, **Karak S**, Moore DJ, Göpfert MC, Jarman AP., Dev Cell. 2012.